# Tower- and Drone-Based BVOC Observations in a Suburban Tokyo Forest: Methodological Insights and MEGAN Comparison~~Long-term BVOC Fluxes in a Suburban Tokyo Forest: Insights from Integrated Drone and Tower Observations~~

Yujiro Ichikawa*[1], Katsuhito Yoshida[2], Shinichi Yonemochi[1], Kentaro Takagi[3], Atsuyuki Sorimachi[2], Kazuhide Matsuda[4], Toshimasa Ohara[5]

[1]Center for Environmental Science in Saitama, 914 Kamitanadare, Kazo City, Saitama, 347-0115, Japan,

[2]Toyo University, 2100 Kujirai, Kawagoe City, Saitama, 350-8585, Japan

[3]Hokkaido Univesity, Aza Tōkanbetsu, Horonobe Town, Teshio District, Hokkaido, 098-2943, Japan

[4]Tokyo University of Agriculture and Technology, 1528 Horinouchi, Hachioji City, Tokyo, 192-0355, Japan

[5]Asia Center for Air Pollution Research, 1182 Sowa Nishi-ku, Niigata City, Niigata, 950-2144, Japan

*Correspondence to*: Yujiro Ichikawa (ichikawa.yujiro@pref.saitama.lg.jp)

**Abstract.** Biogenic volatile organic compounds (BVOCs) substantially ~~impact~~ influence regional photochemical air pollution, ~~global~~ climate ~~change~~, and the carbon cycle. ~~Although research on BVOC emissions is of paramount importance, only few studies have measured long-term BVOC fluxes from forest ecosystems~~However, observational constraints on BVOC emissions from urban or suburban forests in Asian megacity regions under humid subtropical climates remain limited. ~~There are no long-term observational studies on BVOC emissions from suburban forests of major cities in Asia under a humid subtropical climate, which may have a major impact on urban air quality.~~ In this study, w~~W~~e conducted multi-year intermittent~~long-term~~, multi-height BVOC observations at a 30 m flux tower in a suburban Tokyo forest dominated by ~~, evaluating isoprene emission flux from a~~ *Quercus serrata* ~~dominated mixed forest using the aerodynamic gradient method~~. Spatial variability was examined by combining tower measurements with supplemental drone-based sampling. The measurements were compared with estimates from the Model of Emissions of Gases and Aerosols from Nature (MEGAN).~~through integrated drone and tower observations, and Model of Emission Gases and Aerosols from Nature (MEGAN) estimates were compared with measurements.~~ Isoprene volume mixing ratios increased ~~significantly~~ during the warm~~-~~ season observations from ~~(~~May to ~~–~~October~~)~~, accounting for over 90% of the measured BVOC composition during~~in~~ peak summer, while monoterpenes remained low with ~~minimal~~ weak vertical gradients. Isoprene exhibited distinct vertical volume mixing ratio gradients peaking within the canopy, with the daily average emission fluxes ranging from −0.05 to 15.30 mg ~~·~~ m$^{-2}$ ~~·~~ h$^{-1}$. Drone-based measurements indicated horizontal variability in isoprene volume mixing ratios of approximately 10–30% within 30 m of the tower. Flux estimates derived from tower and drone measurements differed by approximately 30%, suggesting that small-scale spatial heterogeneity and height differences can affect gradient-based flux

estimates. ~~Horizontal volume mixing ratio variability within 30 m reached 10–30%, with enhanced heterogeneity in summer. Horizontal flux differed by approximately 30% between tower (height: 23–30 m) and drone (30–40 m) measurements.~~ MEGAN ~~systematically~~ generally overestimated the observed fluxes, particularly during the~~ations with maximum deviations~~ warm-season observations.~~in summer.~~ These results demonstrate the potential of combining tower-based vertical profiling with supplemental drone-based horizontal sampling to evaluate BVOC fluxes and their spatial representativeness. Although the intermittent sampling design limits comprehensive seasonal and interannual interpretations, this study provides methodological insights for future tower- and drone-based BVOC observations and emission model evaluation based on canopy-scale measurements. ~~These findings, derived from long-term observations, will contribute to assessing the impact of BVOCs on air quality and climate in cities worldwide, beyond temperate humid regions of Asia, and to reducing model uncertainties.~~

Keywords: BVOC, Isoprene, Emission, Flux measurements, Drone, Tower, MEGAN

**1. Introduction**

Terrestrial vegetation ~~contributes to the release of~~emits large amounts of biogenic volatile organic compounds (BVOCs), ~~into the atmosphere. BVOCs comprise dozens to hundreds of chemical species,~~ including terpenoids, alkanes, alcohols, carbonyls, esters, ethers, and fatty acids (Penuelas and Llusià, 2004; Yang et al., 2020; Tani and Mochizuki, 2021~~; Yang et al., 2020~~). ~~Although the detailed mechanisms regarding why terrestrial vegetation emit BVOC remain incompletely understood, these compounds are generally thought to be emitted as part of defense systems against abiotic stresses such as heat and biotic stresses such as insects and pathogens (Celedon and Bohlmann, 2019). Furthermore, some studies suggest that BVOC function as signaling molecules for terrestrial vegetation (i.e., allelopathy) to transmit defense signals to surrounding plants when facing biological stress (Ninkovic et al., 2020; Sharifi and Ryu, 2020).~~

~~BVOC emission patterns from terrestrial vegetation vary significantly by species and are broadly categorized into the following four types: Type A, in which BVOC biosynthesis and emission occur simultaneously, is widely observed in broad-leaved trees and herbaceous plants. Type B, in which biosynthesized BVOCs are stored within leaves, branches, and roots before being emitted, is widely observed in conifers and herbaceous plants. Type C exhibits characteristics of both Type A and Type B, while Type D emits little to no BVOCs (Okumura, 2021; Tani and Mochizuki, 2021; Tani et al., 2024). Regarding BVOC emission intensity, Type A species often exhibit both temperature and solar radiation dependences, while Type B species typically show only temperature dependencies.~~

Among ~~the chemical species of BVOCs~~these compounds, terpenoids account for a large proportion of BVOC emissions. Terpenoids primarily include isoprene ($C_5H_8$), monoterpenes ($C_{10}H_{16}$), sesquiterpenes ($C_{15}H_{24}$), and others. The estimated global annual emission of BVOCs is ~1,00~~1~~0~~50~~ Tg~~C~~ ~~·~~yr$^{-1}$, of which isoprene accounts for 535~~03~~ Tg~~C~~ ~~·~~yr$^{-1}$ (~~47~~approximately 50% of the total annual emission) and monoterpenes for 15~~2~~7 Tg~~C~~ ~~·~~yr$^{-1}$ (15~~11~~%) (Guenther et al., ~~1995~~2012). ~~According to estimates based on vegetation type, trees as the primary source account for approximately 821 TgC·yr$^{-1}$ (71% of annual~~



書式変更: インデント : 最初の行 : 0 字

書式を変更: フォントの色 : テキスト 1

書式を変更: フォントの色 : テキスト 1

書式を変更: フォントの色 : テキスト 1

書式を変更: フォントの色 : テキスト 1

書式を変更: フォントの色 : テキスト 1

書式を変更: フォントの色 : テキスト 1

書式を変更: フォントの色 : テキスト 1

書式を変更: フォントの色 : テキスト 1

emission). Needleleaf trees, broadleaf trees, shrubs, grass, and crops each account for 10–30% of the global terrestrial vegetation cover area. Among these, broadleaf trees are estimated to contribute approximately 80% of total BVOC emissions (Guenther et al., 2013).

Many terpenoids exhibit high reactivity with atmospheric reactive species such as hydroxyl radicals (Atkinson and Arey, 2003), with isoprene and monoterpenes having atmospheric lifetimes ranging from tens of minutes to several hours. They significantly contribute to the formation of photochemical pollutants such as tropospheric ozone ($O_3$) and secondary organic aerosols (SOA), thereby affecting air quality, climate, and the carbon cycle (Tani and Kawawata, 2008; OA). $O_3$ and aerosols adversely affect human health and contribute significantly to climate change. Specifically, $O_3$ promotes warming, while aerosols have both absorbing and scattering properties that overall suppress warming (IPCC, 2021). Furthermore, 3–15% of the carbon fixed within plants through photosynthesis is released as isoprene (Tani and Kawawata, 2008). Therefore, improving observational constraints on BVOC emissions from forest ecosystems is important for air quality simulations and emission model evaluation. Thus, BVOCs play a significant role in photochemical air pollution, climate change, and the carbon cycle. Consequently, research on BVOC emissions and atmospheric chemistry is of paramount importance for air quality management and climate change mitigation efforts.

In urban and suburban areas, BVOCs emitted from surrounding forests can influence photochemical air pollution, especially where anthropogenic nitrogen oxides are abundant. Model studies have suggested that BVOC emissions from vegetation surrounding large cities can make non-negligible contributions to ozone formation in urban areas, including the Pearl River Delta (Situ et al., 2013), Berlin (Churkina et al., 2017), and Tokyo (Chatani et al., 2015). These studies indicate that forests located near or upwind of major cities can act as important sources of reactive BVOCs. However, observational information on BVOC emissions from urban and suburban forests remains limited, particularly in Asian megacity regions under humid subtropical climates.

In large urban areas with limited vegetation, one might assume that BVOCs have little or no impact on air quality. Using a model, Situ et al. (2013) found that BVOCs emitted primarily from outside the Pearl River Delta region in China during the autumn of November contributed an average of 7.9 ppb and a maximum of 24.8 ppb to $O_3$ volume mixing ratios in the region, including urban areas downwind. In Berlin, a city renowned for its abundance of green spaces among European cities, the average contribution of BVOCs to $O_3$ was estimated by the model to peak in July, at 17–20% (Churkina et al., 2017). In Japan, it has been reported that approximately 14.1 ppb of the $O_3$ generated in Tokyo during the summer is attributable to BVOCs (Chatani et al., 2015). Furthermore, Nishimura et al. (2015) state that 10.3 ppb (15.9%) of the daily maximum $O_3$ volume mixing ratio in Osaka (Japan's second-largest city after Tokyo) is attributable to BVOCs from forested areas in the surrounding regions. These model studies suggest that forests surrounding major cities may serve as crucial upwind sources of reactive BVOCs. It is, therefore, essential to ascertain the actual emission levels from these forested areas. Research on BVOC emissions from forests plays a crucial role in elucidating the relationship of these emissions with urban air quality. Furthermore, accurate emission data are required to improve the accuracy of model calculations.



**書式を変更:** 蛍光ペン (なし)

**書式を変更:** 蛍光ペン (なし)

**書式を変更:** 蛍光ペン (なし)

**書式を変更:** 蛍光ペン (なし)

Numerical simulation models are ~~primarily~~ used to ~~quantitatively~~ evaluate the impact of chemical emissions on air quality by simulating physicochemical processes ~~mechanisms~~ such as emission, reactions, transport, and deposition. The Model of Emissions of Gases and Aerosols from Nature (MEGAN), which is widely used to estimate BVOC emission fluxes from terrestrial vegetation, uses standardized basal emission rates as an input parameter (Guenther et al., 2006, 2012). However, the ~~majority of~~ basal emission rates are often derived from ~~measurements rely on~~ enclosure measurements ~~methods applied to~~of individual leaves or branches ~~and leaves~~, and scaling these measurements to canopy-scale fluxes can introduce substantial uncertainty because BVOC emissions vary with canopy position, vegetation structure, light environment, temperature, and plant stress.~~and due to the difficulty of accessing different layers of the canopy, they do not fully capture the actual BVOC emissions from the entire tree canopies. In addition, it has been reported that stress factors, such as physical impact or damage to branches or leaves can increase the emission rates of BVOCs (Jutti, 1990), resulting in high measurement uncertainty depending on the conditions used in the enclosure method. Furthermore, considering that basal emission rates vary across canopy layers due to environmental differences (such as temperature and solar radiation), scaling from individual branch and leaf measurements to canopy scale fluxes likely involves significant uncertainty.~~ Micrometeorological methods provide canopy-scale flux estimates without directly disturbing vegetation and are therefore useful for evaluating emission models~~Micro-meteorological methods can directly measure flux within canopy scales. This approach generally utilizes flux towers extending above the upper canopy layer, enabling realistic and reliable measurements without disturbing the vegetation~~ (Guenther et al., 2006; Tani et al., 2024~~; Guenther et al., 2006~~). However, these methods also have important limitations. Flux estimates can be affected by complex canopy structure, terrain, roughness sublayer processes, assumptions regarding turbulent exchange, and chemical loss or transformation within and above the canopy. Therefore, micrometeorological fluxes should be interpreted with consideration of their methodological uncertainty. Complementary approaches, including enclosure measurements, vertical profiling, and spatially distributed sampling, can help constrain these uncertainties. ~~Reportedly, BVOC emissions scaled up from the branch and leaf scales to the canopy scale do not correspond to those obtained using micro-meteorological methods (Bai et al., 2025).~~

Micrometeorological BVOC flux observations have been conducted in various forest ecosystems worldwide~~Numerous studies utilized micro-meteorological methods for BVOC flux observations in various countries and forest types~~ (Fuentes et al., 1999; Fuentes and Wang, 1999; Baker et al., 2005; Holzinger et al., 2006; Ieda et al., 2006; Räisänen et al., 2009; McKinney et al., 2011; Bouvier-Brown et al., 2012; Fares et al., 2013;~~McKinney et al., 2011;~~ Miyama et al., 2013; Situ et al., 2013; ~~Bai et al., 2016;~~ Mochizuki et al., 2014, 2015; Bai et al., 2016; Emmerson et al., 2016; Rantala et al., 2016; Seco et al., 2017; Wei et al., 2018; Mochizuki et al., 2020; Bai et al., 2025; ~~Baker et al., 2005; Bouvier-Brown et al., 2012;~~ Dumont et al., 2026~~; Emmerson et al., 2016; Fares et al., 2013; Fuentes and Wang, 1999; Fuentes et al., 1999; Holzinger et al., 2006; Ieda et al., 2006; McKinney et al., 2011; Miyama et al., 2013; Mochizuki et al., 2014, 2015, 2020; Räisänen et al., 2009; Rantala et al., 2016; Seco et al., 2017; Situ et al., 2013; Wei et al., 2018~~). Nevertheless, observations in urban and suburban forests near Asian megacities remain scarce. In the suburban forest of the Pearl River Delta region, Situ et al. (2013) measured BVOC fluxes using the relaxed eddy accumulation method from a 37 m tower; however, the observations were conducted

書式を変更: 蛍光ペン (なし)

for only several days during October–December 2010. Additional case studies are therefore needed to evaluate BVOC fluxes and model performance in suburban forest environments under humid subtropical conditions.

Most tower-based flux observations are conducted at a single fixed location, and their spatial representativeness is often difficult to assess. This issue is particularly relevant in heterogeneous forests, where vegetation structure, canopy height, and local meteorology can vary over short horizontal distances. Drone-based sampling provides a promising supplementary approach for examining horizontal variability around fixed towers. Although drone observations cannot replace tower measurements because of limited flight duration and sampling time, they can provide useful information on small-scale spatial heterogeneity and help interpret uncertainties in gradient-based flux estimates.

Although recent studies on BVOC emphasize the need to understand actual seasonal variations in BVOC emissions (Chatani et al., 2022) and to conduct long-term flux observations (Bai et al., 2025; Tani and Mochizuki, 2021), many flux observations conducted worldwide are limited to periods ranging from a few days to less than a year, resulting in a lack of seasonal or annual assessments, making the results unrepresentative. Very few long-term observations of BVOC fluxes using towers have been conducted for more than a year (e.g., Bouvier-Brown et al., 2012; Dumont et al., 2026; Rantala et al., 2016). In Japan, only Mochizuki et al. (2014) conducted a one-year monoterpene flux observation in the *Larix kaempferi* forest at the Fuji Hokuroku Flux Research Site. Although long-term flux measurements using micro-meteorological methods at BVOC emission sources in suburban areas are crucial for gaining a better understanding of and estimating the impact of BVOCs on urban air quality, such studies are extremely rare. Rantala et al. (2016) conducted flux measurements for over a year in the background forest area of Helsinki, Finland, which has a subarctic climate. However, to the best of our knowledge, no such studies have been conducted in the suburbs of major cities in Asia under a humid subtropical climate. Therefore, in this study, we conducted observations over a long period of two and a half years in a forest area in the suburbs of Tokyo, to clarify the actual BVOC emission levels. As scientific knowledge regarding BVOC emissions from forested areas in suburban settings is relevant not only in Japan but also in similar environments around the world, this study serves as an important case study. Furthermore, most flux observations rely on single fixed towers, with limited assessment of spatial representativeness and horizontal heterogeneity, particularly in complex suburban forest environments.

In this study, we conducted intermittent multi-year, multi-height BVOC observations at a 30 m flux tower in a suburban Tokyo forest dominated by *Quercus serrata* from June 2023 to October 2025.This study involved multi-height observations of BVOCs and measured emission flux using the aerodynamic gradient method (AGM), one of the micrometeorological techniques, at a flux tower installed in a research forest in the Tokyo metropolitan area, Japan, located within a humid subtropical climate zone, over a period of approximately two and a half years, from June 2023 to October 2025. Isoprene emission fluxes were estimated using the aerodynamic gradient method. Drone-based measurements were conducted on selected days as a supplementary approach to examine horizontal variability near the tower and to evaluate the spatial representativeness of the tower observations. The observed fluxes were also compared with MEGAN estimates to assess model-observation agreement and possible sources of discrepancy. The objectives of this study were to: (1) characterize BVOC volume mixing ratios and isoprene fluxes observed by multi-height tower measurements during the intermittent

**書式を変更:** フォント : 斜体

sampling campaign, (2) evaluate small-scale horizontal variability using supplementary drone-based measurements, and (3) examine the agreement and discrepancies between observed isoprene fluxes and MEGAN estimates. Through these analyses, this study provides methodological insights into tower- and drone-based BVOC observations in suburban forest environments.By integrating aerial observations using multi-rotor unmanned aerial vehicles (UAV, commonly known as drones) with fixed-point observations around the flux tower, we further assessed the spatial variability of measurements obtained from a single flux tower. In addition, by comparing the observational data with estimates from the MEGAN model, we evaluated model performance and characterized sources of uncertainty. Comparative analyses between long-term observational data from suburban areas and the MEGAN model are rare, making these findings particularly valuable. The uniqueness of this study lies in the fact that it involved long-term, on-site assessments of the temporal and spatial variability of BVOCs in suburban forest areas, which directly affect urban air quality, as well as comparisons between model predictions and observed datasets. Specifically, we address three key questions: (1) What is the seasonal and interannual variability of BVOC emissions in a suburban Tokyo Forest? (2) What is the magnitude of spatial heterogeneity in BVOC volume mixing ratios and fluxes? (3) How well does MEGAN reproduce observed emissions, and what are the primary sources of model-observation discrepancy?

## 2. Methods

### 2.1 Site description

This study was conducted at the Field Museum Tamakyuryo (FM Tama), a research forest facility of Tokyo University of Agriculture and Technology located in the western suburb of Tokyo (35°38′18″N, 139°22′41″E), as shown in Fig. S1. A 30 m high scaffold flux tower has been constructed on the forest floor atof FM Tama (168 m above sea level). This site has been extensively used to conduct numerous atmospheric observational and micro-meteorological studies (e.g., Matsuda et al., 2015; Xu et al., 2021). Details regarding the FM Tama are described in Matsuda et al. (2015);, they but are briefly outlined below. The site covers approximately 20 hectares. The area around the flux tower is dominated by the deciduous tree *Quercus serrata*, and the needleleaf tree *Japanese cedar* is also sparsely scattered in small numbers throughout other parts of the site, creating a mixed forest character. The trees reach heights of approximately 20 m, with the canopy layer distributed between 10–20 m above ground level. *Q. serrata* began to grow lush foliage around April and had shed its foliage by around November to December. In contrast, *J. cedar* is an evergreen tree and generally does not shed its leaves. The *J. cedar* trees at FM Tama are estimated to be approximately 50 years old (Naemura et al., 2003), and the *Q. serrata* trees are also presumed to be roughly the same age.

The wind rose for the observation period described in Section 2.2 is shown in Fig. S2. Prevailing winds are were predominantly southerly, followed by northerly winds and, then easterly winds, with westerly winds being rare. Together with the surrounding land use, this wind pattern suggests that BVOCs measured at the flux tower were mainly influenced by emissions from FM Tama under the sampled conditions. However, possible contributions from nearby vegetation outside the research forest cannot be completely excluded. Naganuma Park, a forest park, lies west of the flux tower, but westerly winds were infrequent during the observation period~~Consequently, the wind rose indicates that no major BVOC emission sources exist upstream outside the research forest, suggesting that the BVOC components detected at the flux tower primarily originate from FM Tama. Meanwhile, although Naganuma Park, a forest park, lies west of the flux tower, its influence is considered negligible~~.

### 2.2 Observation design and sampling period~~Sampling period~~

BVOC sampling was conducted intermittently from~~conducted for 1–3 days each month from~~ June 2023 to October 2025.~~,~~ Measurements were typically performed for 1–3 d per month, except during periods when sampling could not be conducted because of equipment maintenance, power outages, or unsuitable weather conditions. Rainy days were excluded from the analysis. In total, BVOC samples were collected on 34 sampling days during the study period.~~though there were months when measurements could not be performed due to equipment maintenance or power outages.~~ The observation dates and representative meteorological ~~data for those days are shown in~~conditions are summarized in Table S1~~; rainy days are not included~~. ~~In this paper, a~~All times are expressed in Japan~~ese~~ S~~s~~tandard T~~t~~ime (JST, UTC+9).

Sampling was typically conducted using 30 min integrated sorbent tube samples, mainly during 10:00–12:00 and 14:00–16:00. During supplemental drone-based observations described in Section 2.6, the sampling duration was shortened to 15 or 17 min to fit within the available drone flight time and operational constraints. When samples were missing within 10:00–16:00 observation period, daily averages were calculated only from available paired observations. Note that these daily averages do not represent full diurnal averages.

The sampling design was intended to obtain multi-height BVOC observations under selected daytime conditions over multiple years, rather than to provide continuous flux measurements. Therefore, the dataset should be interpreted as multi-year intermittent observations. Monthly, seasonal and interannual features discussed in this study represent tendencies observed under the sampled conditions and should not be regarded as a complete climatology of BVOC emissions at the site. The main objectives of the observational design were to accumulate data and insights into tower-based BVOC flux measurements in a suburban forest, to examine the spatial representativeness of fixed-point observations using supplemental drone-based sampling,  and to compare the observed isoprene fluxes with MEGAN estimates.

### 2.3 Meteorological observations

A three~~3~~-dimensional ultrasonic anemometer (YOUNG, 81000) installed at the ~~flux tower top of~~ 30 m tower top measured horizontal and vertical wind directions and speed, as well as virtual temperature, and data were averaged over 10–30 min intervals. Additionally, an integrated weather sensor (VAISALA, WXT520) was installed at the flux tower heights of 25 m, 20 m, 17 m, and 1 m from June 2023 to November 30, 2023, and at 30 m, 24 m, 20 m, 17 m, 10 m, and 2 m between ~~from~~ February 22, 2024 and~~to~~ October 2025 to measure air temperature, relative humidity, and horizontal wind direction and speed (Climatec CVS-HMP110 thermo-hygrometers and Climatec CYG-91000 anemometers were also used for some periods). The 10~~-~~-min averages were used to obtain vertical profiles of each parameter. In cases where meteorological data could not be acquired at the flux tower due to maintenance or other reasons, measurements from the nearest Hachioji air quality monitoring station, which is managed by the Tokyo ~~metropolitan~~ Metropolitan ~~government~~Government, were used.

Solar radiation including photosynthetic photon flux density (PPFD) was measured at 10 ~~-~~min intervals using a pyranometer (PREDE, PCM-01N) at 30 m height on~~f~~ the flux tower. The leaf area index (LAI) around the tower was measured for 1–3 d per month using a plant canopy analyzer (LI-COR LAI-2200). LAI was measured at four-fixed locations around the tower, and the average value of these locations was used. Therefore, LAI represents local canopy conditions around the tower rather than those of the entire FM Tama.~~from multiple locations was used.~~

### 2.4 BVOC sampling and measurement

Based on the previously reported BVOC measurement conditions (Ichikawa et al., 2023), isoprene and seven monoterpenes (α/β-pinene, camphene, myrcene, 3-carene, limonene, p-cymene) were selected as target substances for measurement. BVOC samples were collected using an in-house sampling device as shown in Fig. S3. Air samples entering through the atmospheric inlet passed through a dehumidification tube (FUJIFILM Wako Pure Chemical, magnesium perchlorate, elemental analysis grade, 6–14 mesh) and an ozone scrubber cartridge (FUJIFILM Wako Pure Chemical, Presep-C Ozone Scrubber, potassium iodide). The air was then divided into four flow paths using a PTFE manifold. Each flow path was connected to a sorbent tube, with a two-way solenoid valve connected downstream. The opening and closing of the valves were controlled by a ~~4~~four-channel timer, enabling sample collection at different time intervals. All tubing was made of PTFE and the flow rate was set to 100 mL ~~-~~min$^{-1}$.

The sampling devices were installed at heights of 30 ~~m~~ and 23 m above ~~the canopy top~~ground level, above the main canopy layer, at 17 m within the canopy, and at 3 m near the forest floor~~ground level~~, as shown in Fig. 1 (a). Sampling was generally conducted between 10:00–16:00 using 30 min integrated sorbent tube samples; typically, four samples were collected in the morning and four in the afternoon. ~~Sampling was conducted with a time resolution of 10–30 min during the period from 10:00 am – 4:00 pm (JST), typically four samples in the morning and four in the afternoon.~~

書式を変更: フォントの色 : テキスト 1
書式を変更: フォントの色 : テキスト 1
書式を変更: フォントの色 : テキスト 1
書式を変更: フォントの色 : テキスト 1
書式を変更: フォントの色 : テキスト 1

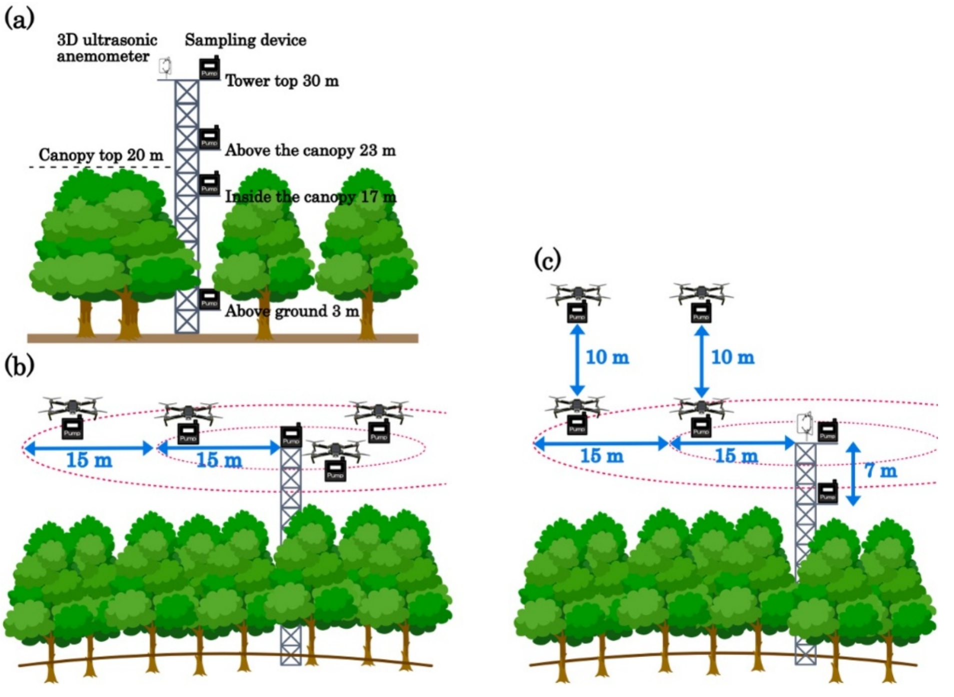
(a)
3D ultrasonic anemometer
Sampling device
Tower top 30 m
Above the canopy 23 m
Canopy top 20 m
Inside the canopy 17 m
Above ground 3 m
(b)
15 m
15 m
(c)
10 m
10 m
15 m
15 m
7 m

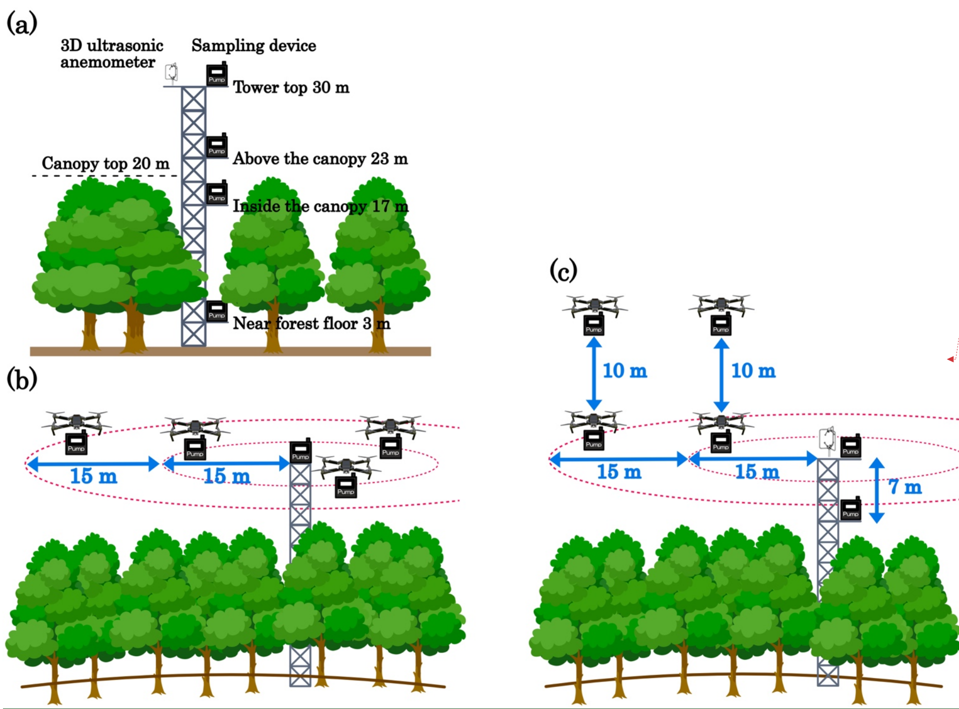


**Figure 1: Schematic diagram showing the configuration of sampling equipment on the drone and flux tower, along with the observation points. (a) Observation method at multiple heights on the tower; (b) mMethod for observing horizontal volume mixing ratio variations using the tower and drone; (c) mMethod for observing horizontal flux variations using the tower and drone.**

書式変更: 左揃え

書式を変更: フォント : 9 pt, 太字

書式を変更: フォント : 9 pt, 太字

For the sorbent tube, Air Toxics (Camsco, multibed type packed with Carbograph and Carbosieve) was used from June 2023 to May 2024, and a manufacturer customized multibed type packed with Tenax TA and Carbotrap B (Camsco) was used from June 2024 to October 2025. Conditioning of the sorbent tubes was performed with a temperature program of 40°C (hold 1 min) →10°C·min$^{-1}$→350300°C (60 min) in a thermostatic chamber modified from a gas chromatography oven while high-purity nitrogen gas (>99.9999% purity) was flowing at a flow rate of 50 mL ·min$^{-1}$. Immediately after conditioning, the sorbent tubes were tightly closed at both ends with a brass cap using PTFE sealer, placed in stainless-steel containers with activated carbon, and stored in a glass desiccator under vacuum until sampling.

After sample collection, the sorbent tubes were tightly capped at both ends with brass caps, sealed in a desiccator with activated carbon to prevent contamination in an air-conditioned, controlled room, and stored until further analysis. Sample measurement was performed within one 1 month of sampling.

Field blanks were used to evaluate potential contamination during transport, storage, field handling, and exposure associated with the sampling procedure. For each sampling campaign, blank sorbent tubes were transported to the field together with the sample tubes. During sampling preparation and after sample collection, the field blank tubes were uncapped and recapped at the same time as the sample tubes. During active sampling, the field blank tubes were kept capped and placed near the active sampling tubes. The field blanks were subsequently transported, stored, and analyzed in the same manner as the actual samples. The blank values were subtracted from the measured values of the corresponding samples. These field blanks were then transported, stored, and measured in the same manner as the actual samples. The blank values were subtracted from the measured values of the corresponding samples. As the field blanks were not connected to the active sampling line, possible contamination or losses within the inlet and sampling line were not fully evaluated.

Preliminary recovery experiments were conducted to evaluate potential losses of the target BVOCs associated with the dehumidification tube and ozone scrubber cartridge. The recovery rates ranged from 64% to 129% among the target compounds: 87% for isoprene, 99% for α-pinene, 101% for camphene, 102% for myrcene, 64% for β-pinene, 79% for 3-carene, 71% for limonene, and 129% for p-cymene. Although most compounds showed recoveries within approximately 70%–130%, β-pinene showed relatively lower recovery of 64%.A travel blank was used to confirm the effects of contamination during sample transport and storage. The travel blank was analyzed using the same method as that for the actual samples, and its value was subtracted from the analysis value of the actual samples.

Based on the static dilution method described in the U.S. EPA published manual "TO-15A" (EPA, 2019), a fixed amount of each BVOC component standard solution dissolved in methanol (FUJIFILM Wako Pure Chemical, LCMS grade) was spiked into a clean inert stainless-steel -vacuum canister (GL Sciences, GL-Scan). The canister was then heated at 60°C for 2 h to completely vaporize the components. After returning to room temperature, the canister was pressurized with VOC-free high-purity nitrogen gas (>99.9999% purity) to create a BVOC mixed standard gas. Toluene-$d_8$ (FUJIFILM Wako Pure Chemical, NMR grade, 99.5% purity) was used as the internal standard gas and was prepared in the same manner as described above.

BVOCs were analyzed using a gas chromatography–mass spectrometer (GC-MS; Shimadzu, GC-MS QP2010plus) connected to an automated thermal desorption system (PerkinElmer, TurboMatrix 650 ATD). Detailed measurement conditions are as described in a previous study (Ichikawa et al., 2023). These devices undergo regular manufacturer inspections to ensure that they are in good condition and free of defects. The lower detection limit (3σ) was calculated from the standard deviation (σ) obtained from repeated measurements of the standard gas (*n*=5–7).

## 2.5 Flux calculation using the aerodynamic gradient method

書式変更: インデント : 最初の行 : 1 字

According to Tani et al. (2024), *Q. serrata* emits isoprene but does not emit monoterpenes. As shown in the Section 3.1 below, volume mixing ratio of monoterpenes remained extremely low compared to isoprene, and sometimes fell below the detection limits. Considering that isoprene emission around the flux tower is primarily attributable to the dominant species *Q. serrata*, flux calculations were performed for isoprene only.

The aerodynamic gradient method (AGM) adopted in this study to determine isoprene emission flux is a ~~fundamental method classically used to estimate flux of trace gas components~~micrometeorological method used to estimate fluxes of trace gases. The flux calculation in AGM is defined by~~ the following~~ Eq. (1) in accordance with Fick~~'~~'s first law (Erisman and Draaijers 1995; Fuentes, 1999; Räisänen, T. et al., 2009; Hayashi, 2010;~~,~~ Matsuda et al., 2010).

書式を変更: 蛍光ペン (なし)

$$F_{\mathrm{obs}} = -K \cdot \frac{\partial C}{\partial z} = -\frac{u_* \cdot \kappa \cdot (C_{\mathrm{u}} - C_{\mathrm{l}})}{ln\left(\frac{z_{\mathrm{u}} - d}{z_{\mathrm{l}} - d}\right) - \Psi_{\mathrm{h}}\left(\frac{z_{\mathrm{u}} - d}{L}\right) + \Psi_{\mathrm{h}}\left(\frac{z_{\mathrm{l}} - d}{L}\right)} \quad (1)$$

where, $F_{obs}$ is the observed flux (mg ~~·~~m$^{-2}$ ~~·~~h$^{-1}$), $K$ is the eddy diffusion coefficient (m$^2$ ~~·~~s$^{-1}$), $C$ represents concentration (µg ~~·~~m$^{-3}$), $z$ represents height (m), and the subscripts u and l denote two heights above the canopy (u > l). $u_*$ is the friction velocity (m ~~·~~s$^{-1}$), κ is the empirically determined von Kármán ~~Karman~~ constant (=0.41), $\Psi_h$ is the integrated stability correction for heat, $L$ is the Monin–~~-~~Obukhov length~~,~~ and $d$ is the displacement height (m). $u_*$ and $L$ were derived from micro~~-~~meteorological elements (e.g., horizontal and vertical wind speed, virtual temperature). The value of $d$ was derived from the vertical wind profile measured at the FM Tama flux tower by Xu et al. (2021) (April–November: 16 m, December–March: 15 m).

Sampling was conducted primarily between 10:00 and 16:00 because the AGM is less suitable under stable nighttime or early morning conditions with weak turbulence~~Observations in this study were not conducted at night or in the early morning for the following considerations, and were primarily carried out between 10:00 am–4:00 pm. AGM is generally not suitable for atmospheric conditions with stable boundary layers and weak turbulence during nighttime or early morning hours, whereas daytime implementation is preferable when turbulence intensifies and vertical flows and concentration gradients emerge~~ (Erisman and Draaijers 1995; Tani et al., 2024). During the observation period, t~~T~~he average and ~~(~~median~~)~~ friction velocities~~ty~~ for the entire period ~~was~~ were 0.64 and ~~(~~0.60~~)~~ m ~~·~~s$^{-1}$~~.~~, respectively, and n~~N~~o data points fell below ~~the threshold of~~ 0.10 m ~~·~~s$^{-1}$, a threshold used by ~~which~~ Räisänen et al. (2009) to ~~exclud~~excluded~~ed from analysis as~~ weak~~-~~ turbulence conditions~~intensity~~. These results indicate that turbulence was generally sufficient during the sampling period~~This indicates that sufficient turbulence intensity was maintained during 10:00 am–4:00 pm, and the prerequisites for the AGM were generally satisfied~~. However, it should be noted that flux estimates based on AGM are subject to uncertainties associated with the concentration gradient, the eddy diffusion coefficient, the stability correction, and the assumption that the selected measurement height lies within a layer of approximately constant flux.~~Furthermore, since the emission of many BVOC components exhibit temperature and light dependence, emissions are higher during the day, with isoprene showing this tendency most prominently. Note that due to maintenance of the observation equipment, some data are missing from December 1, 2023, to February 22, 2024.~~

**2.6 Supplemental dDrone-based measurements**

Supplemental drone-based measurements were This study utilizedconducted using a multi-rotor drone (DJI, Matrice 350 RTK) to evaluate the spatial representativeness of tower-based BVOC measurements under selected observational conditions. .The drone was used as a supplementary platform for short-duration horizontal sampling around the tower, rather than as a replacement for continuous tower observations.Multi-rotor drone offers the advantages of vertical takeoff and landing (VTOL) capability without requiring a runway, stable hovering, excellent maneuverability, and lower operational costs compared to helicopters or airplanes. Furthermore, the majority of aircraft are equipped with lithium polymer (Li-Po) batteries, and it is extremely important that they do not emit any exhaust gases that could significantly impact atmospheric observation data. One disadvantage of atmospheric observation using drones is that, given current battery technology, flight times are limited to approximately 15–30 min when considering the payload of meteorological and atmospheric observation equipment and cameras mounted on the aircraft.

The swirling airflow generated by propeller rotation can causes atmospheric turbulence around the aircraft. If the placement of sample intake ports and measurement devices is not carefully considered, this turbulence may affectsignificantly impacts measurement accuracy and precision. However, it has been pointed outnoted that many previous studies using drones do not address countermeasures for this swirling airflow (Altamira-Colado et al., 2024). Based on computational results from a fluid model by McKinney et al. (2019) and verification results from preliminary tests experiment using thean actual aircraft regarding swirling airflow, the sample inlet, dehumidification tube, ozone scrubber cartridge and sorbent tube were mounted on a titanium based support extendinged approximately above the aircraft (approximately 60 cm above the the maindrone body of aircraft), as shown in Fig. 2. This configuration was designed to reduce the influence of propeller induced airflow and aircraft vibration on the sampled air.minimizes the effects of swirling airflow and aircraft vibration on the sample.

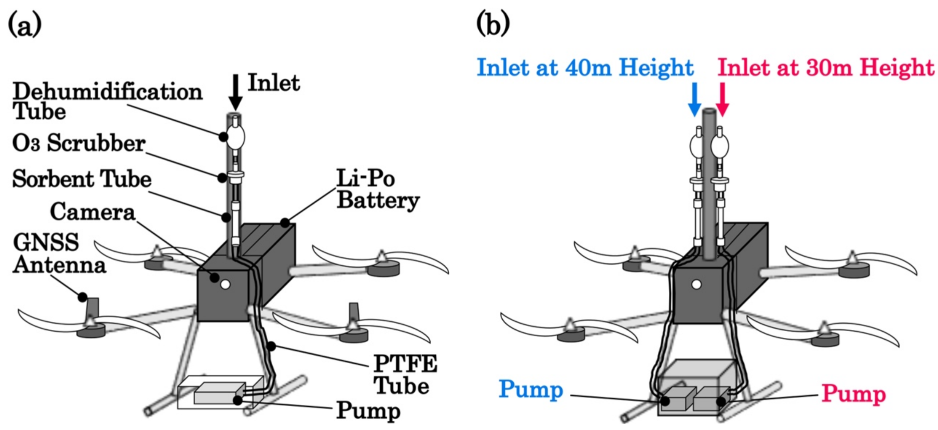


**Figure 2: Status of equipment installed for BVOC sampling using a drone. (a) Installation for horizontal volume mixing ratio variations, and (b) ~~i~~Installation for horizontal flux variations.**

On October 12, 2023, July 23, 2024, and June 17, 2025, simultaneous tower and drone measurements were conducted at 30 m height. As shown in Fig.1 (b), the drone sampled air at four locations approximately 15–30 m from the tower at different azimuths to evaluate horizontal variability in BVOC volume mixing ratios. The flight position was determined by acquiring positional data via the Global Navigation Satellite System (GNSS) antenna~~,~~ and was ~~also constantly monitored~~ visually monitored from the~~ flux~~ tower. After arriving at each~~the~~ observation point, the drone~~aircraft~~ hovered briefly ~~for a while to ensure~~to stabilize~~ty~~ before ~~initiating~~ sampling was initiated using the pump timer function. The stability of the drone at its fixed position during hovering is shown in Fig. S4. The drone equipment mounting method for these observations is ~~as~~ shown in Fig. 2 (a), and each sampling period lasted 15 min. ~~and the observation time was set to 15 min.~~ The flight altitude was precisely measured relative to the tree canopy using its onboard altitude sensor.

On July 29, 2025, an additional drone experiment was conducted to examine the sensitivity of gradient-based flux estimates to sampling location and height intervals, as shown in Fig. 1(c). Drone samples were collected at 30 and 40 m, and fluxes were calculated using the AGM equation in the same manner as for the tower observations. The configuration of equipment installed for this observation is shown in Fig. 2 (b), which carried two pumps and other equipment. Due to safety concerns, the drone did not collect samples at altitudes below 30 m, so the altitude differs from that of the tower. ~~The configuration of equipment installed for this observation is shown in Fig. 2 (b), carrying two pumps and other equipment.~~ After completing the first sampling at a height of 30 m at the observation point, the aircraft ascended vertically to 40 m and performed another sampling. As the drone payload limit prevented the installation of a three-dimensional ultrasonic

書式を変更: 蛍光ペン (なし)
書式を変更: 蛍光ペン (なし)
書式を変更: 蛍光ペン (なし)
書式を変更: 蛍光ペン (なし)

anemometer, micrometeorological parameters measured at the tower were used for the drone-based flux calculation. This calculation assumes that the tower and drone sampling heights were influenced by similar micrometeorological conditions and that the selected height interval was suitable for a gradient-based flux estimate. As the same tower-derived micrometeorological parameters were used for the tower- and drone-based AGM calculations, differences between the tower- and drone-derived flux estimates mainly reflect differences in the measured concentration gradients and sampling height intervals. However, possible horizontal differences in turbulence caused by local canopy roughness, terrain, or flow distortion could not be evaluated. Therefore, drone-derived fluxes should be interpreted as an exploratory assessment of spatial representativeness and methodological uncertainty under tower-derived turbulence conditions, rather than as an independent quantitative validation of the tower-based fluxes.

For the autumn season on October 12, 2023, and for the summer seasons on July 23, 2024, and June 17, 2025, parallel observations were conducted at the same height (30 m) using the drone and the flux tower at four locations approximately 15–30 m horizontally away from the flux tower (with differing azimuths), as shown in Fig. 1 (b), to evaluate the variability in volume mixing ratio in the horizontal direction. The flight position was determined by acquiring positional data via the Global Navigation Satellite System (GNSS) antenna, and was also constantly monitored visually from the flux tower. After arriving at the observation point, the aircraft hovered for a while to ensure stability before initiating sampling using the pump timer function. The stability of the drone at its fixed position during hovering is shown in Fig. S4. The drone equipment mounting method for these observations is as shown in Fig. 2 (a), and the observation time was set to 15 min. The flight altitude was precisely measured relative to the tree canopy using its onboard altitude sensor.

Furthermore, on July 29, 2025, during the summer season, spatial variability of the emission flux was evaluated using drone and flux tower, as shown in Fig. 1(c). Specifically, we calculated flux using the AGM equation presented in Section 2.5, based on observation results from two drone heights (30 m and 40 m) and two heights at flux tower (23 m and 30 m). Due to safety concerns, the drone did not collect samples at altitudes below 30 m, so the altitude differs from that of the tower. The drone had weight restrictions, preventing the installation of a 3-dimensional ultrasonic anemometer. Therefore, this study utilized data obtained from the flux tower, based on the assumption of the gradient method that both observation heights belong to the constant flux layer, and that there are no significant differences in micro-meteorological parameters. The configuration of equipment installed for this observation is shown in Fig. 2 (b), carrying two pumps and other equipment. After completing the first sampling at a height of 30 m at the observation point, the aircraft ascended vertically to 40 m and performed another sampling.

### 2.7 MEGAN calculation and model evaluationIsoprene emission estimation model

書式変更: インデント : 最初の行 : 0 字

We compared the tower-based observed isoprene emission fluxes with model calculations from MEGAN (Guenther et al., 2006, 2012), an extensively used BVOC emission estimation model, to evaluate model–observation agreement under the sampled conditionsto evaluate its applicability and reproducibility. MEGAN calculations were conducted at a 10 min time resolution for the daytime period from 10:00–16:00 for each day from June 1, 2023 to October 31, 2025. Thus, the model was run continuously for the daytime sampling window throughout the study period, rather than only for the individual observation days. For comparison with the observations, model outputs corresponding to the actual sorbent tube sampling times were extracted and paired with the observed fluxes.~~The calculation period for this study was set from June 1, 2023 to October 31, 2025 to cover the actual observational period.~~ Additionally,

PPFD, meteorological variables,~~elements~~ and LAI data were obtained as described ~~by the method described~~ in Section 2.3. The comparison therefore represents model–observation agreement during the sampled daytime periods and should not be interpreted as an evaluation of full-day emission estimates.~~We estimated isoprene emission from *Q. serrata* at a 10-min time resolution.~~ The estimation of isoprene emission flux $F_{\mathrm{cal}}$ (mg m$^{-2}$ h$^{-1}$) was performed using the following Eq. (2), with parameters set based on the original literature for MEGAN (Guenther et al., 2006, 2012).

$$F_{\mathrm{cal}} = \varepsilon \cdot \gamma_P \cdot \gamma_T \cdot \gamma_{LAI} \cdot \gamma_{age} \cdot \gamma_{SM} \cdot \gamma_{\mathrm{CO_2}} \cdot \rho \quad (2)$$

where, $\varepsilon$ is the basal emission rate under standard conditions for the plant functional type (PFT), and we adopted the standard value of 10 mg m$^{-2}$ h$^{-1}$ for isoprene from broadleaf deciduous temperate trees. The standard conditions for MEGAN are described in Guenther et al. (2006, 2012); for example, a leaf temperature of 30°C, PPFD of 1500 μmol m$^{-2}$ s$^{-1}$, and a standard canopy structure ($LAI_{std}$) of 5. ~~Note that while a~~Although a PPFD of 1000 μmol m$^{-2}$ s$^{-1}$ ~~was~~is typically used as the standard condition at the leaf level in~~for~~ the G93 algorithm~~model~~ (Guenther et al., 1993), MEGAN uses~~a PPFD of~~ 1500 μmol m$^{-2}$ s$^{-1}$ ~~is~~at the ~~used in MEGAN at the~~ canopy scale. ~~Furthermore, t~~The $\gamma$ terms~~variables~~ represent activity factors related to ~~various~~ environmental and phenological conditions, where $\gamma_P$ ~~represents~~ for light ~~dependency~~response, $\gamma_T$ ~~represents~~ for temperature ~~dependency~~response, $\gamma_{LAI}$ ~~represents~~ for LAI, $\gamma_{age}$ for~~represents~~ leaf age, $\gamma_{SM}$ for~~represents~~ soil moisture response, and $\gamma_{CO_2}$ ~~cor~~for~~responds to the~~ carbon dioxide response. ~~$\rho$ represents T~~The escape efficiency $\rho$, which is the proportion of isoprene emitted from the canopy that escapes into the upper atmosphere, was set to ~~and the value of~~ 0.96 following ~~was used~~ Guenther et al. (2006). The settings of the activity factors used in this study are described below. ~~The setting of activity factors related to environmental conditions used in MEGAN is explained in the supplement S1.~~

### 2.7.1 Activity factor for light response $\gamma_P$

The light dependent activity factor $\gamma_P$ was calculated every 10 min using Eqs. (3) – (5).

$$\gamma_P = 0 \text{ for } \sin(a) < 0 \quad (3a)$$

$$\gamma_P = \sin(a)\left\{2.46 \cdot \left[1 + 0.005 \cdot \left(P_{daily} - 400\right)\right] \cdot \phi - 0.9 \cdot \phi^2\right\} \text{ for } \sin(a) > 0 \quad (3b)$$

$$\phi = \frac{P_{\mathrm{ac}}}{\left(\sin(a) \cdot P_{\mathrm{toa}}\right)} \quad (4)$$

$$P_{\mathrm{toa}} = 3000 + 99 \cdot \cos\left(2 \cdot 3.14 \cdot \frac{(DOY - 10)}{365}\right) \quad (5)$$

where, $a$ is solar angle (degrees), $P_{daily}$ is daily average above canopy PPFD (μmol m$^{-2}$ s$^{-1}$), $\varphi$ is the above canopy PPFD transmission factor (non-dimensional), $P_{ac}$ is the above canopy PPFD (μmol m$^{-2}$ s$^{-1}$), $P_{toa}$ is PPFD at the top of the

書式を変更: フォント : 斜体
書式を変更: 下付き
書式を変更: フォント : 斜体
書式を変更: 下付き
書式を変更: フォント : 斜体
書式を変更: フォント : 斜体
書式を変更: 下付き
書式を変更: 上付き
書式を変更: 上付き
書式を変更: フォント : 斜体
書式変更: インデント : 最初の行 : 0 字
書式を変更: フォント : 斜体
書式を変更: 下付き
書式を変更: 上付き
書式を変更: 上付き
書式を変更: フォント : 斜体
書式を変更: 下付き

atmosphere (μmol $m^{-2}$ $s^{-1}$), and DOY is the day of year. The solar angle $\beta$ was calculated from the latitude of FM Tama, the solar declination, and the hour angle.

#### 2.7.2 Activity factor for temperature response $\gamma_T$

The temperature dependent activity factor $\gamma_T$ was calculated using Eqs. (6) – (9).

$$\gamma_T = \frac{E_{\mathrm{opt}} \cdot C_{T2} \cdot \exp(C_{T1} \cdot \chi)}{\{C_{T2} - C_{T1} \cdot [1 - \exp(C_{T2} \cdot \chi)]\}} \qquad (6)$$

$$\chi = \frac{\left[\left(\frac{1}{T_{\mathrm{opt}}}\right) - \left(\frac{1}{T_{\mathrm{hr}}}\right)\right]}{0.00831} \qquad (7)$$

$$E_{\mathrm{opt}} = 1.75 \cdot \exp\left(0.08 \cdot \left(T_{\mathrm{daily}} - 297\right)\right) \qquad (8)$$

$$T_{\mathrm{opt}} = 313 + 0.6 \cdot \left(T_{240} - 297\right) \qquad (9)$$

where, $T_{hr}$ is the hourly average air temperature (K), $T_{daily}$ is the daily average air temperature (K), $E_{opt}$ is the maximum normalized emission capacity, $T_{opt}$ is the temperature at which $E_{opt}$ occurs, $T_{240}$ is the average air temperature over the past 240 h (K), and $C_{T1}$ (=80 kJ $mol^{-1}$) and $C_{T2}$ (=200 kJ $mol^{-1}$) are empirical coefficients that represent the energies of activation and deactivation, respectively (Guenther et al., 1999, 2006). For calculating 10 min values of $\gamma_T$, the hourly average air temperature corresponding to each model time step was used as $T_{hr}$. The temperature history term $T_{240}$ was calculated from continuous meteorological data over the preceding 240 h, rather than from daytime data only. This allowed $\gamma_T$ to account for antecedent thermal conditions before each daytime model time step.

#### 2.7.3 Activity factor for LAI $\gamma_{LAI}$

The activity factor for LAI, $\gamma_{LAI}$, was estimated using Eq. (10).

$$\gamma_{LAI} = \frac{0.49 \cdot LAI}{\sqrt{1 + 0.2 \cdot LAI^2}} \qquad (10)$$

As LAI was measured intermittently, the LAI value from the closest observation date was used for each model calculation day.

#### 2.7.4 Activity factor for leaf age $\gamma_{age}$

The leaf age activity factor $\gamma_{age}$ was estimated using Eq. (11).

$$\gamma_{\mathrm{age}} = F_{\mathrm{new}} \cdot A_{\mathrm{new}} + F_{\mathrm{gro}} \cdot A_{\mathrm{gro}} + F_{\mathrm{mat}} \cdot A_{\mathrm{mat}} + F_{\mathrm{old}} \cdot A_{\mathrm{old}} \qquad (11)$$

where $F$ represents the proportion of leaves in each age class, $A$ denotes the leaf age-specific activity factor, and the subscripts new, gro, mat, and old indicate new, growing, mature, and old leaves, respectively. The values for $A$ for isoprene are summarized in the table presented by Guenther et al. (2012), with $A_{new}$=0.05, $A_{gro}$=0.6, $A_{mat}$=1.0, and $A_{old}$=0.9.

**書式を変更:** 上付き
**書式を変更:** 上付き
**書式を変更:** フォント : 斜体
**書式を変更:** フォント : 斜体
**書式を変更:** 下付き
**書式変更:** インデント : 最初の行 : 0 字
**書式を変更:** フォント : 斜体
**書式を変更:** 下付き
**書式を変更:** フォント : 斜体
**書式を変更:** 下付き
**書式を変更:** フォント : 斜体
**書式を変更:** 下付き
**書式を変更:** フォント : 斜体
**書式を変更:** 下付き
**書式を変更:** フォント : 斜体
**書式を変更:** 下付き
**書式を変更:** フォント : 太字 (なし)
**書式変更:** インデント : 最初の行 : 1 字
**書式を変更:** フォント : 斜体
**書式を変更:** 下付き

Based on field observations of *Q. serrata* at FM Tama, the leaves emergence generally occurred between April to May, mature leaves dominated from June to mid-September, leaf coloration and senescence occurred from mid-October to November, and leaves were mostly absent from December to March. Based on these local phenological observations, the monthly fractions of each leaf age class were set as shown in Table S2. As *Q. serrata* is deciduous and leaves were mostly absent from December to March, $\gamma_{age}$ was set to 0 during this period.

### 2.7.5 Activity factors for soil moisture $\gamma_{SM}$ and carbon dioxide $\gamma_{CO2}$

Soil moisture data (volumetric water content, m³/m³) were obtained from ERA5-Land (Muñoz-Sabater et al., 2021), a land surface dataset provided by the European Centre for Medium-Range Weather Forecasts. Soil moisture varies significantly with depth, and whether plants can absorb water depends on root depth (Guenther et al., 2006). We calculated weighted daily averages of soil moisture content at a spatial resolution of 0.1° for three soil layers (layer 1: 0–7 cm, layer 2: 7–28 cm, layer 3: 28–100 cm) around FM Tama. The calculated values ranged from 0.17–0.43 $m^3\ m^{-3}$. Based on these values, we assumed that severe soil moisture stress was unlikely during the calculation period and $\gamma_{SM}$ was set to 1.

As the area surrounding FM Tama is residential, $CO_2$ concentrations during the observation period are expected to show no significant variation from those in the general atmospheric environment. Therefore, the influence of $CO_2$ on isoprene emissions was assumed to be constant. Therefore, $\gamma_{CO_2}$ was set to 1 for the entire period.

### 2.7.6 Comparative evaluation of observed and MEGAN calculated values

The correspondence and error characteristics between~~ the obtained calculated value~~ $F_{cal}$ and ~~the observed isoprene emission flux~~ $F_{obs}$ were ~~evaluate~~evaluated~~d~~. To calculate the degree of systematic overestimation or underestimation of the model, the mean bias error~~ bias~~ (M~~E~~BE) was determined using Eq. (12~~3~~).~~ as follows:~~

$$\mathrm{MBE} = \frac{1}{N}\sum_{i=1}^{N}(F_{cal,i} - F_{obs,i}) \qquad (12)$$

where $N$ is the number of data points used for comparison. A positive MBE ~~value~~ indicates ~~that~~ model that the overestimates, whereas ~~the observed values, while~~ a negative MBE ~~bias~~ indicates model underestimation.

Furthermore, as a comprehensive indicator for evaluating the magnitude of model error, the root mean square error (RMSE) was calculated using Eq. (13~~4~~).~~ as follows:~~

$$\mathrm{RMSE} = \sqrt{\frac{1}{N}\sum_{i=1}^{N}(F_{cal,i} - F_{obs,i})^2} \qquad (13)$$

The closer this statistical indicator approaches its minimum value of 0, the closer the calculated value ~~approaches~~ is to the actual measured value.

書式を変更: 蛍光ペン (なし)
書式を変更: フォント : 斜体
書式を変更: フォント : 斜体
書式を変更: 下付き
書式を変更: フォント : 斜体
書式を変更: 下付き
書式変更: インデント : 最初の行 : 1 字
書式を変更: 上付き
書式を変更: フォント : 太字
書式変更: インデント : 最初の行 : 0 字

As the observations were intermittent and limited to selected daytime periods, these statistics were used to evaluate model–observation differences under the sampled conditions rather than for assessing full seasonal model performance.

## 3. Results

### 3.1 Volume mixing ratio of BVOCsBVOC composition during the intermittent sampling campaign

Fig. S53 shows the monthly average volume mixing ratios of the eight target BVOC species at each sampling height during the intermittent sampling campaign. The corresponding numerical values are summarized in Table S3. The averages reported in this section are based on samples collected between 10:00 and 16:00 on the observation days.shows the stacked bar graph of the monthly average volume mixing ratios of eight BVOC components by height over a 3-year period. The numerical data for each component in each month are summarized in Table S2. Note that the average values mentioned in the following text refer to the period from 10:00 am–4:00 pm on the observation day.

From November to April, volume mixing ratios of all target compounds were generally low at all heights. In contrast, from May to October, isoprene volume mixing ratios increased markedly, with several samples exceeding 10,000 pptv during July and August. During peak summer observations, isoprene accounted for more than 90% of the measured BVOC composition at all heights (Fig. S6). From November to April, volume mixing ratios of all components were generally low throughout the month, with no significant differences observed at different heights. Conversely, during the warmer period from May to October, isoprene volume mixing ratios exhibited extremely high levels, with differences also observed at different heights.

書式を変更: 蛍光ペン (なし)

書式を変更: 蛍光ペン (なし)

書式を変更: 蛍光ペン (なし)

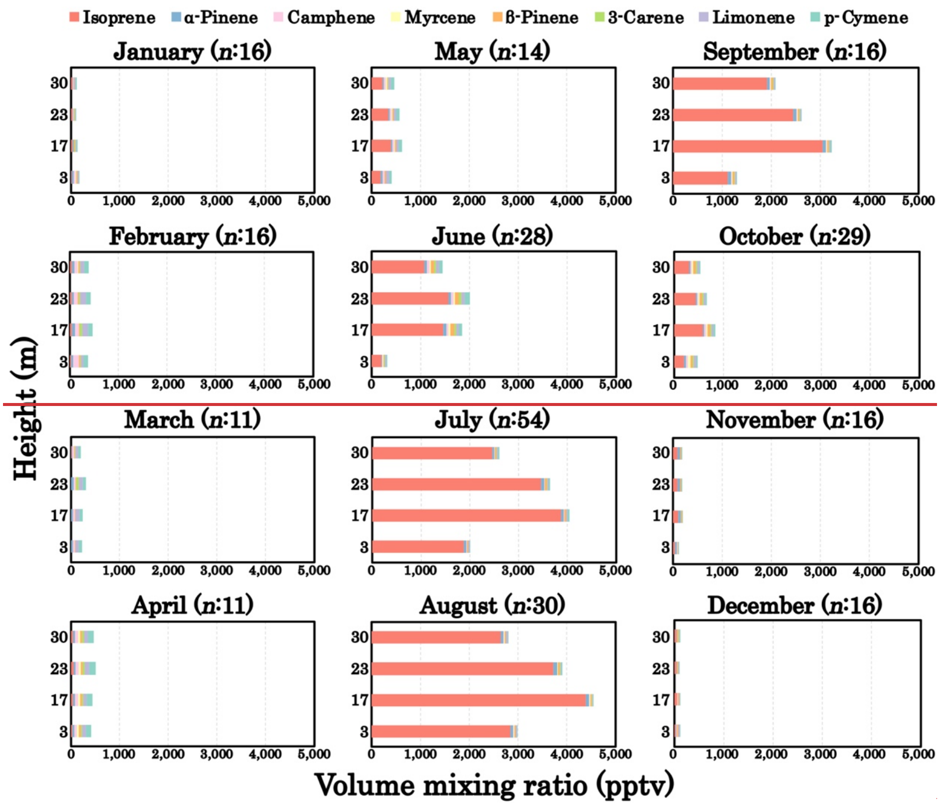


**Figure 3: Stack bar chart of monthly average volume mixing ratios (pptv) of eight BVOC components by height over a 3-year period.**

書式変更: インデント : 最初の行 : 1 字

Isoprene volume mixing ratios began rising in May, peaking around July to August, with multiple samples exceeding 10,000 pptv. Fig. S5 shows the composition ratios of each component at different heights for each month. In July and August, isoprene accounted for over 90% of the total volume mixing ratio at all heights. Although the detailed mechanisms underlying isoprene emission in plants remain incompletely understood, the widely accepted explanation is that it protects leaves from high temperatures (Sharkey et al., 2008). This study also observed a tendency for isoprene volume mixing ratios to increase during periods of high temperature.rising temperatures over the long observation period. As detailed in Section 3.2, an isoprene volume mixing ratio gradient forms between the canopy interior and exterior from this period onward.

Monoterpene volume mixing ratios were much lower than those of isoprene throughout the campaign.~~Monoterpenes do not exhibit seasonal variations as pronounced as isoprene. While slight increases may be observed during summer, isoprene tends to dominate the volume mixing ratio to the overall composition.~~ Among the measured, ~~g~~ monoterpenes, α-pinene, limonene, and p-cymene ~~showed~~ were relatively ~~high volume mixing ratios~~abundant, but each ~~component~~ generally accounted for only about 1–2% of the total measured BVOC volume mixing ratio during ~~the~~ summer observations. Distinct vertical gradients of monoterpenes were not evident.~~, and the formation of volume mixing ratio gradients with height was also unclear.~~ These~~is~~ results are consistent with previous reports that ~~corresponds with Tani et al. (2024), indicating that~~ *Q. serrata* is primarily an isoprene-emitting species and emits few ~~but releases almost no~~ monoterpenes (Tani et al., 2024).

Therefore, the following sections focus on isoprene.~~Through long-term atmospheric observations around the FM Tama flux tower, isoprene was confirmed to be a major component. Therefore, the following sections will focus on isoprene.~~

**3.2 Vertical profiles of isoprene**

Figure~~.~~ 34 shows the vertical distribution of isoprene volume mixing ratios at different heights~~ for each month from January to December, using box plots and average values~~. The boxes represent the 25th–75th percentile ranges, the whiskers represent the 2nd–98th~~8~~ percentile ranges, and the median and average are overlaid.

書式を変更: フォント : (英) Times New Roman
書式を変更: フォント : (英) Times New Roman
書式を変更: 蛍光ペン (なし)
書式を変更: 蛍光ペン (なし)
書式を変更: 蛍光ペン (なし)

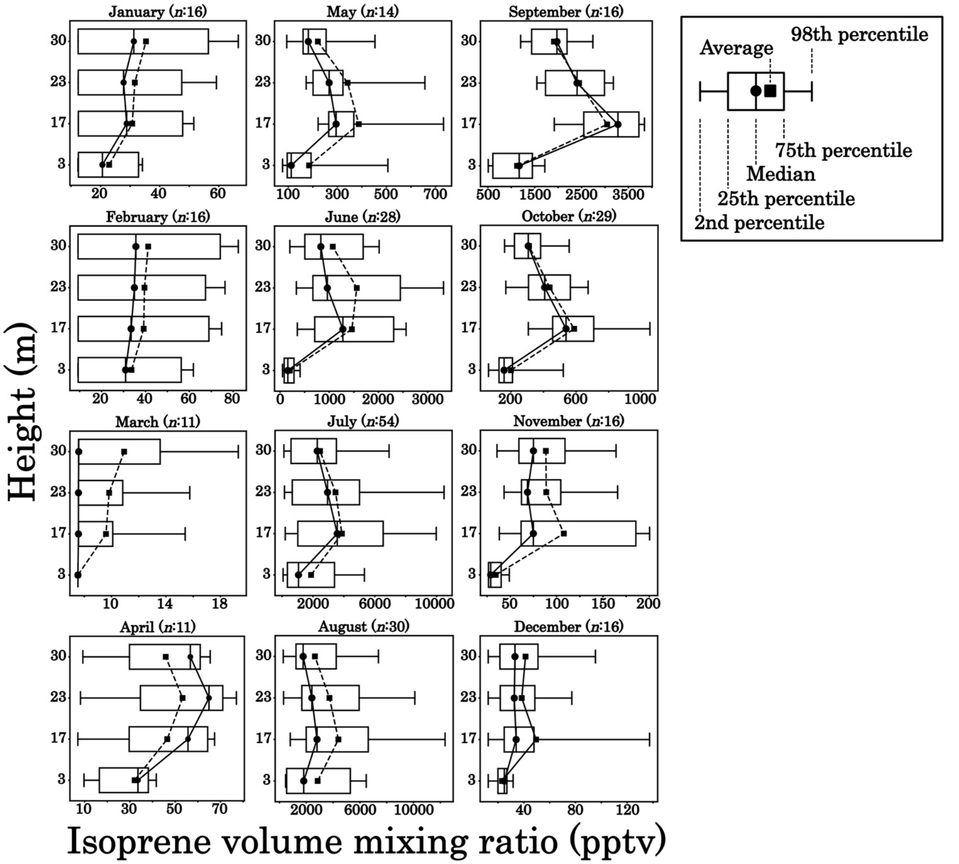


**Figure 34: Boxplots overlaid with average values for showing the monthly and seasonal distribution of isoprene volume mixing ratios by height during the intermittent sampling campaign.over a 3-year period. The solid and dashed lines connect the median and average values for each height, respectively.**

During the warm-season observations (May to September), when *Q. serrata* leaves were densely foliated, isoprene volume mixing ratios were generally highest at 17 m, corresponding to the canopy layer. The distributions at 17 m showed higher upper-percentile values than those at the other heights, indicating thatthe primaryenhanced isoprene volume mixing ratios were frequently observed within the canopy, source of isoprene emissions was located within the height range where *Q. serrata* leaves were concentrated (the canopy range of 10–20 m). At 23 and 30 m, above the main canopy layer, the distributions also showed extended upper tails during the warm-season, suggesting upward transport of isoprene emitted from the canopy. In contrast, isoprene volume mixing ratios at 3 m near the forest floor were generally lower and showed narrower distributions.

During the cold-season observations (December to April), isoprene volume mixing ratios were low at all heights, and clear vertical gradients were not evident. These results indicate that the vertical structure of isoprene was most apparent during the foliated warm-season period.

The median and average values tended to be highest at 17 m, corresponding to the canopy interior, for many months. Particularly during the warm season (May to September) when *Q. serrata* leaves were densely foliated, the distribution at 17 m shifted toward higher volume mixing ratios (positive skewness), as evident from the x-axis scale of isoprene volume mixing ratios. This directly reflects that the primary source of isoprene emissions was located within the height range where *Q. serrata* leaves were concentrated (the canopy range of 10–20 m). At 23 m and 30 m above the canopy, an increase in upper percentile values and a tendency toward a longer right tail in the distribution were also observed during the warm season. This suggests the existence of events where isoprene emitted from within the canopy is transported upward, leading to temporary high volume mixing ratios. Meanwhile, at 3 m, corresponding to the forest floor level, the median and average values were relatively lower throughout the year compared to other heights, and the distribution range was relatively narrower. This suggests that the primary source of isoprene emissions is located within the canopy rather than at the forest floor. During the cold season (December to April), the distribution range narrowed across all heights. This reflects a state of significantly suppressed isoprene emissions, likely attributable to low temperatures, reduced solar radiation, and the phenology of *Q. serrata* leaf fall.

To more clearly illustrate seasonal variations, Fig. 4 also shows the vertical distribution of isoprene for each season. The seasons are defined as follows: December through February is winter, March through May is spring, June through August is summer, and September through November is autumn. During winter, isoprene volume mixing ratios were extremely low at all heights, with a narrow distribution range. The median and average values were nearly identical, indicating low skewness in the distribution. Furthermore, no significant vertical gradient was observed between 17, 23, and 30 m heights. These results reflect a state where isoprene emission from *Q. serrata* was significantly low.

In spring, increases in the average values were observed at 17 m and a distinct vertical structure began to form compared to winter. Particularly at 17 m, the upper percentile values were higher than those at other heights, suggesting that the primary source of isoprene emission resided within the canopy. In contrast, volume mixing ratios at 3 m remained low with a narrow distribution range, indicating a limited contribution from the forest floor.

During summer, isoprene volume mixing ratios reached their highest levels among the four seasons. At 17 m, both the median and average reached their maximum values, with the entire distribution significantly shifted toward higher volume

**書式変更:** インデント : 最初の行 : 0 字

~~mixing ratios. At 23 m and 30 m, the distributions clearly showed a positive skew with a long right tail in the distribution. This reflects that isoprene generated within the canopy is emitted as a net amount and undergoes vertical transport.~~

~~In autumn, although isoprene volume mixing ratios decreased than that in summer, a vertical structure centered around 17 m was observed. The median and average values were higher than those in the following winter, and the skewness of the distribution also persisted. This indicates that although emission flux levels decreased with the drop in temperature and the onset of leaf fall, the primary source height for isoprene emission from within the canopy was maintained, a trend particularly pronounced in September (autumn season). Meanwhile, the upper percentile values at 23 m and 30 m in autumn were less pronounced than those in summer, suggesting a decrease in the high emission events.~~

書式変更: インデント : 最初の行 : 1 字

### 3.3 Tower-based i~~I~~soprene emission flux ~~observed at the tower~~observations and environmental relationships

#### ~~3.3.1 Trend over two and a half years based on observed values~~

Figure ~~5~~ 4 shows the daily average isoprene emission fluxes ($F_{obs}$) calculated ~~based on~~from the vertical gradient of isoprene concentration ~~($\partial C/\partial z$) and the diffusion coefficient ($K$)~~between ~~at heights of~~ 23 ~~m~~ and 30 m. Canopy temperature and PPFD during the observation days are also shown in Fig. 4~~Additionally, temperature inside the canopy, and PPFD during the observation period are overlaid (Fig. 5)~~. The daily average values and~~±~~ standard deviations for $F_{obs}$ and related meteorological parameters are summarized in Table 1.~~,~~ ~~with~~ $F_{obs}$ ranged~~ing~~ from −0.05 to 15.30 mg·m⁻²·h⁻¹ ~~.~~during the observation period.

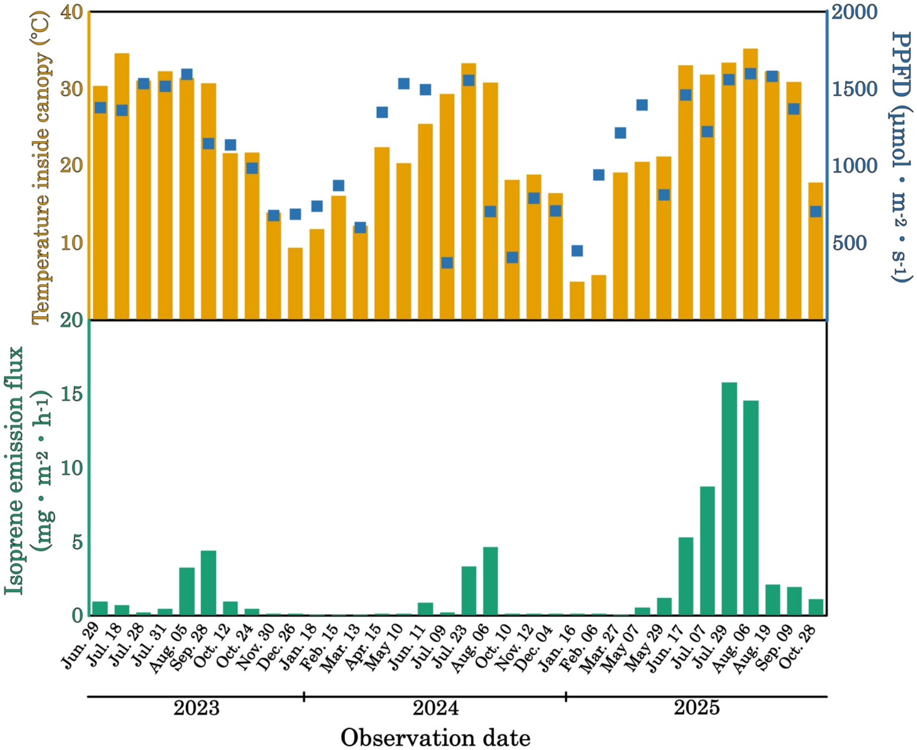


**Figure 45:** Daily average isoprene emission fluxes estimated from tower-based measurements (green bar graph), together with canopy temperature (orange bar graph) and PPFD (blue filled square) during the observation days from June 2023 to October 2025. Fluxes were calculated from the concentration gradient between 23 and 30 m using the aerodynamic gradient method. Isoprene emission flux $F_{obs}$ (green bar graph), temperature inside canopy (orange bar graph), and PPFD (red filled square) for observation days from June 2023 to October 2025.

**Table 1.** Monthly Daily averages of **isoprene emission flux, friction velocity, diffusion coefficient, canopy temperature, PPFD, and LAI during the observation** days.period

| Year | Month | Day | $F_{obs}$ (mg m$^{-2}$ h$^{-1}$) | $u^*$ (m s$^{-1}$) | $K$ (m$^2$ s$^{-1}$) | Canopy Temp. (°C) | PPFD (µmol m$^{-2}$ s$^{-1}$) | LAI |
|---|---|---|---|---|---|---|---|---|

書式付きの表

| | | | Ave. | ± | Std. | Ave. | ± | Std. | Ave. | ± | Std. | Ave. | ± | Std. | Ave. | ± | Std. | Ave. | ± | Std. |
|---|---|---|---|---|---|---|---|---|---|---|---|---|---|---|---|---|---|---|---|---|
| 2023 | Jun. | 29 | 0.95 | ± | 0.70 | 0.46 | ± | 0.05 | 0.48 | ± | 0.19 | 30.4 | ± | 1.3 | 1360 | ± | 639 | 2.80 | ± | 0.44 |
| | Jul. | 18 | 0.63 | ± | 0.86 | 0.62 | ± | 0.10 | 0.58 | ± | 0.13 | 34.6 | ± | 0.6 | 1340 | ± | 447 | 2.67 | ± | 0.52 |
| | Jul. | 28 | 0.21 | ± | 0.85 | 0.85 | ± | 0.21 | 0.66 | ± | 0.03 | 31.1 | ± | 1.0 | 1513 | ± | 376 | 3.19 | ± | 0.43 |
| | Jul. | 31 | 0.43 | ± | 0.28 | 0.83 | ± | 0.22 | 0.65 | ± | 0.06 | 32.2 | ± | 0.2 | 1497 | ± | 403 | 3.19 | ± | 0.43 |
| | Aug. | 5 | 3.21 | ± | 2.55 | 1.03 | ± | 0.28 | 0.74 | ± | 0.09 | 31.4 | ± | 0.9 | 1577 | ± | 304 | 2.94 | ± | 0.58 |
| | Sep. | 28 | 4.22 | ± | 3.95 | 0.52 | ± | 0.13 | 0.59 | ± | 0.15 | 30.7 | ± | 1.7 | 1127 | ± | 398 | 2.77 | ± | 0.63 |
| | Oct. | 12 | 0.92 | ± | 0.68 | 0.47 | ± | 0.17 | 0.61 | ± | 0.17 | 21.6 | ± | 0.7 | 1116 | ± | 469 | 2.85 | ± | 0.43 |
| | Oct. | 24 | 0.45 | ± | 0.20 | 0.41 | ± | 0.13 | 0.57 | ± | 0.16 | 21.7 | ± | 0.7 | 967 | ± | 427 | 3.42 | ± | 0.47 |
| | Nov. | 30 | 0.01 | ± | 0.06 | 0.62 | ± | 0.25 | 0.67 | ± | 0.11 | 13.9 | ± | 1.4 | 656 | ± | 420 | 2.23 | ± | 0.63 |
| | Dec. | 26 | 0.00 | ± | 0.03 | 0.77 | ± | 0.17 | 0.67 | ± | 0.07 | 9.4 | ± | 0.7 | 668 | ± | 326 | 2.36 | ± | 0.22 |
| 2024 | Jan. | 18 | -0.05 | ± | 0.05 | 0.44 | ± | 0.10 | 0.66 | ± | 0.14 | 11.8 | ± | 1.3 | 717 | ± | 269 | 1.98 | ± | 0.58 |
| | Feb. | 15 | -0.02 | ± | 0.03 | 0.78 | ± | 0.25 | 0.65 | ± | 0.08 | 16.1 | ± | 1.3 | 853 | ± | 341 | 1.58 | ± | 0.35 |
| | Mar. | 13 | -0.04 | ± | 0.06 | 1.40 | ± | 0.15 | 1.10 | ± | 0.09 | 12.2 | ± | 0.7 | 579 | ± | 374 | 1.02 | ± | 0.21 |
| | Apr. | 15 | 0.08 | ± | 0.06 | 0.81 | ± | 0.29 | 0.73 | ± | 0.06 | 22.5 | ± | 0.9 | 1329 | ± | 467 | 1.59 | ± | 0.07 |
| | May | 10 | 0.08 | ± | 0.06 | 0.81 | ± | 0.29 | 0.73 | ± | 0.06 | 20.4 | ± | 0.1 | 1513 | ± | 379 | 3.06 | ± | 0.63 |
| | Jun. | 11 | 0.83 | ± | 0.35 | 0.91 | ± | 0.15 | 0.66 | ± | 0.05 | 25.4 | ± | 0.4 | 1474 | ± | 462 | 2.25 | ± | 0.46 |
| | Jul. | 9 | 0.25 | ± | 0.40 | 0.25 | ± | 0.07 | 0.10 | ± | 0.05 | 29.3 | ± | 0.5 | 350 | ± | 243 | 2.91 | ± | 0.62 |
| | Jul. | 23 | 3.26 | ± | 2.60 | 0.58 | ± | 0.09 | 0.51 | ± | 0.07 | 33.3 | ± | 0.8 | 1537 | ± | 425 | 3.16 | ± | 0.79 |
| | Aug. | 6 | 4.53 | ± | 4.60 | 0.45 | ± | 0.08 | 0.38 | ± | 0.10 | 30.8 | ± | 0.9 | 684 | ± | 284 | 3.02 | ± | 0.42 |
| | Oct. | 10 | 0.09 | ± | 0.10 | 0.77 | ± | 0.08 | 0.46 | ± | 0.09 | 18.2 | ± | 0.5 | 385 | ± | 212 | 2.56 | ± | 0.44 |
| | Nov. | 12 | 0.01 | ± | 0.10 | 0.59 | ± | 0.14 | 0.52 | ± | 0.14 | 18.9 | ± | 0.7 | 772 | ± | 415 | 2.52 | ± | 0.50 |
| | Dec. | 4 | 0.00 | ± | 0.00 | 0.78 | ± | 0.17 | 0.65 | ± | 0.14 | 16.5 | ± | 0.5 | 686 | ± | 363 | 2.19 | ± | 0.14 |
| 2025 | Jan. | 16 | 0.00 | ± | 0.00 | 0.60 | ± | 0.09 | 0.62 | ± | 0.09 | 5.0 | ± | 0.8 | 429 | ± | 106 | 1.33 | ± | 0.15 |
| | Feb. | 6 | 0.00 | ± | 0.00 | 0.72 | ± | 0.12 | 0.70 | ± | 0.07 | 5.8 | ± | 1.1 | 922 | ± | 320 | 1.03 | ± | 0.27 |
| | Mar. | 27 | 0.00 | ± | 0.01 | 0.63 | ± | 0.13 | 0.49 | ± | 0.20 | 19.1 | ± | 1.3 | 1195 | ± | 422 | 1.50 | ± | 0.22 |
| | May | 7 | 0.56 | ± | 0.11 | 1.05 | ± | 0.11 | 0.72 | ± | 0.10 | 20.5 | ± | 0.8 | 1376 | ± | 555 | 3.02 | ± | 0.82 |
| | May | 29 | 1.14 | ± | 1.07 | 0.48 | ± | 0.06 | 0.38 | ± | 0.07 | 21.2 | ± | 0.6 | 793 | ± | 388 | 2.17 | ± | 0.41 |
| | Jun. | 17 | 5.11 | ± | 3.75 | 0.53 | ± | 0.13 | 0.51 | ± | 0.10 | 33.1 | ± | 0.6 | 1443 | ± | 510 | 2.83 | ± | 0.75 |
| | Jul. | 7 | 8.43 | ± | 10.85 | 0.42 | ± | 0.19 | 0.46 | ± | 0.15 | 31.9 | ± | 0.4 | 1205 | ± | 366 | 3.06 | ± | 0.49 |
| | Jul. | 29 | 15.30 | ± | 9.34 | 0.56 | ± | 0.17 | 0.52 | ± | 0.10 | 33.4 | ± | 0.9 | 1538 | ± | 417 | 2.88 | ± | 0.37 |
| | Aug. | 6 | 14.02 | ± | 15.33 | 0.53 | ± | 0.18 | 0.54 | ± | 0.04 | 35.3 | ± | 0.3 | 1579 | ± | 305 | 2.92 | ± | 0.62 |
| | Aug. | 19 | 2.04 | ± | 1.93 | 0.54 | ± | 0.11 | 0.54 | ± | 0.03 | 32.3 | ± | 0.7 | 1563 | ± | 180 | 2.92 | ± | 0.62 |
| | Sep. | 9 | 1.90 | ± | 3.02 | 0.49 | ± | 0.16 | 0.49 | ± | 0.08 | 30.9 | ± | 0.7 | 1350 | ± | 293 | 2.83 | ± | 0.53 |
| | Oct. | 28 | 1.04 | ± | 0.60 | 0.38 | ± | 0.10 | 0.38 | ± | 0.18 | 17.9 | ± | 0.9 | 684 | ± | 343 | 2.74 | ± | 0.44 |

~~The daily average showed clear seasonal variation throughout the observation period.~~ Positive isoprene fluxes were mainly ~~was~~ observed ~~from mid-April~~ during the warm~~-~~ season sampling days, especially from ~~with significant fluxes occurring from~~ June to September~~,~~. Fluxes were generally low during the cold-season observations and during early spring. ~~and a tendency for fluxes to subside around October. Young leaves have been reported to have lower isoprene emission capacity than mature leaves (Kuzma and Fall, 1993), and a similar trend is observed in *Q. serrata*. Consequently, in April, when young leaves were abundant, relatively low emission flux levels were observed, whereas, from November to March the emission flux levels decreased, showing low values on most days.~~

High fluxes were observed on several summer sampling days, particularly in 2025. As the sampling was intermittent and meteorological conditions differed among observation days, these differences should be interpreted as variations among sampled summer conditions rather than indicating an interannual trend. Possible meteorological controls are discussed in Section 4.1.~~High emission flux levels were observed from June to August, and the period averages (medians) were 1.2 (0.6) mg·m$^{-2}$·h$^{-1}$ in 2023, 2.0 (1.0) mg·m$^{-2}$·h$^{-1}$ in 2024, and 9.2 (5.2) mg·m$^{-2}$·h$^{-1}$ in 2025. As shown, 2025 exhibits a tendency toward higher flux levels than other years. As meteorological factors are considered one cause, further explanation will be provided in Section 4.1.~~

Figure S7 shows the relationships between the isoprene flux and canopy temperature, PPFD, and LAI using the unaveraged dataset (*n*=263).

**書式を変更:** 蛍光ペン (なし)

~~**3.3.2 Correlation analysis of isoprene flux and meteorological parameters**~~

**書式変更:** インデント : 最初の行 : 1 字

~~The trend pattern of isoprene flux, which begins to rise in spring, peaks in summer, and declines toward the end of autumn, was consistently repeated each year over the approximately 3-year observation period, suggesting that isoprene flux depends on variations in temperature and photosynthetically active radiation (PPFD), as well as the phenology of *Q. serrata*. Next, we analyzed the correlation between isoprene fluxes and these factors. Figure 6 shows a two-dimensional scatter plot based on the entire unaveraged dataset (*n*=263) for atmospheric temperature within the canopy height (17 m), PPFD, and LAI.~~ As isoprene emissions exhibit exponential or saturated nonlinear ~~relationships with~~responses to temperature, PPFD, and LAI (Guenther et al., 1993, 2006; Yu et al., 2017), ~~we considered the possibility of nonlinear responses and performed analyses using~~ Spearman's rank correlation coefficient ($r_s$) was used.

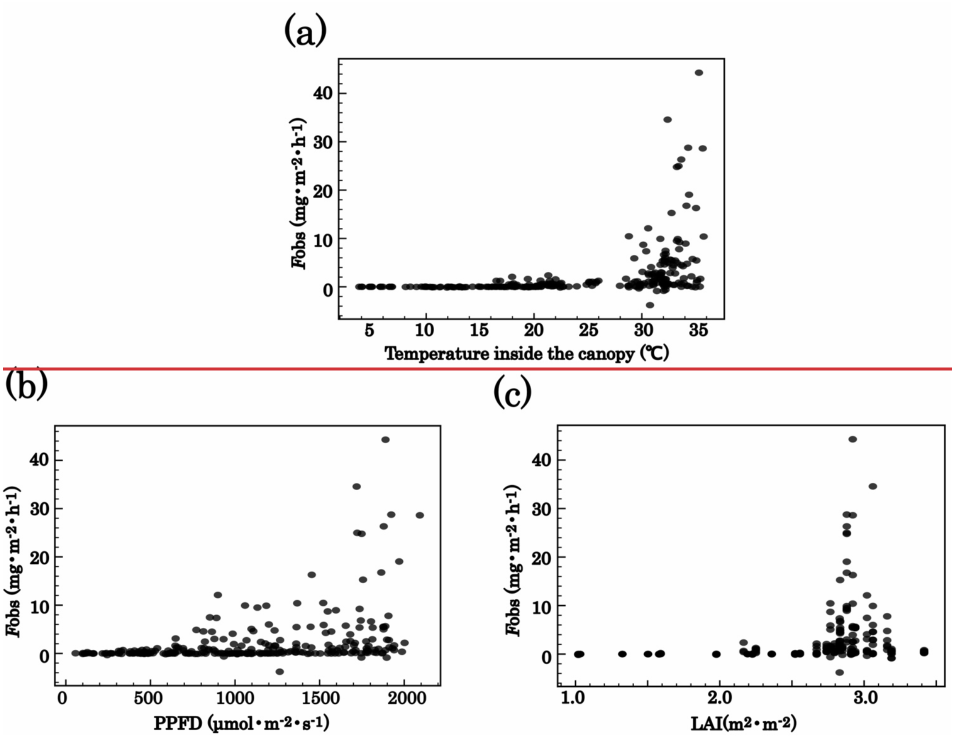


~~**Figure 6: Two-dimensional scatter plots of isoprene emission flux versus various environmental factors: (a) temperature inside the canopy, (b) PPFD, and (c) LAI. Pink squares indicate spring plots, green circles indicate summer plots, orange diamonds indicate autumn plots, and blue triangles indicate winter plots.**~~

~~The results showed that c~~Canopy temperature ($r_s$=0.71, $p$ < 0.001), PPFD ($r_s$=0.49, $p$ < 0.001), and LAI ($r_s$=0.58, $p$ < 0.001) showed positive monotonic relationships with isoprene flux~~exhibited strong or moderately monotonically increasing relationships with isoprene emissions~~. These relationships are consistent with the known temperature, light, and phenological controls on isoprene emissions. However, because the dataset was obtained from intermittent daytime sampling, these correlations should be interpreted as relationships within the sampled conditions rather than as a comprehensive characterization of seasonal or interannual controls.

To further examine the combined effects of temperature and light, we also examined the relationship among $F_{obs}$, canopy temperature, and PPFD using a three-dimensional scatter plot (Fig. S8). Under high temperature and high PPFD conditions,

**書式変更:** インデント : 最初の行 : 0 字

**書式を変更:** フォント : 斜体

**書式を変更:** 下付き

$F_{obs}$ tended to be high. However, some data points showed relatively low $F_{obs}$ even when both canopy temperature and PPFD were high. This result indicates that temperature and light were important drivers of isoprene flux under the sampled daytime conditions, but they did not fully explain the observed flux variability. To analyze the factors involved, we first calculated the 75th percentile (Q3) for both temperature and PPFD from the entire observation dataset (n=263). We then extracted data points simultaneously satisfying temperature ≥ Q3 (approximately 32°C) and PPFD ≥ Q3 (approximately 1571 μmol $m^{-2}$ $s^{-1}$). The $F_{obs}$ distribution of this subset (n=37) was classified as follows. L-$F_{obs}$ denotes the group below the 25th percentile (approximately 1.5 mg $m^{-2}$ $h^{-1}$, n=10), and corresponds to the data points marked with black circles in Fig. S8. Although we were unable to identify a clear cause for the occurrence of L-$F_{obs}$, other factors, such as canopy-scale source distribution, local light environment, turbulent transport, concentration-gradient uncertainty, and tower-footprint representativeness, may also have contributed to the variability in $F_{obs}$.

Isoprene production is significantly influenced by synthetic substrates (e.g., dimethylallyl diphosphate) generated by photosynthesis within chloroplasts and by isoprene synthase. Photosynthesis is PPFD dependent, and the activity of isoprene synthase is known to be strongly affected by temperature (Rasulov et al., 2010; Chen et al., 2022). Therefore, it is considered that isoprene emissions correlate with temperature and PPFD. According to Rasulov et al. (2010), the pool size of dimethylallyl diphosphate varies with temperature and decreases under high temperature conditions exceeding a threshold, suggesting that elevated temperatures may influence isoprene emission rates. Guenther et al. (1993) observed the relationship between isoprene emissions and leaf temperature in isoprene emitting trees—Sweetgum, Eucalyptus, Aspen, and Velvet bean. They reported that, depending on the tree species, the emission peak shifted around 35°C, with emission levels decreasing above approximately 40°C. Exceeding the threshold temperature is thought to be associated with the inactivation of the synthetic substrate. The highest temperature recorded during this observation period was 35.7°C, indicating that air temperatures (not leaf temperatures, but considered to be proportional) likely reached levels near the emission peak. Further analysis of isoprene emission, temperature, and PPFD is described in following Section 4.1. LAI is expected to have a positive correlation with isoprene emissions, but once LAI reaches a certain level, emission saturates due to limitations in light availability (Yu et al., 2017).

### 3.4 Supplemental dDrone-based observations of horizontal variability

#### 3.4.1 Horizontal variation variability in in isoprene volume mixing ratio around the flux towers

Supplemental drone-based measurements were used to examine short-range horizontal variability in isoprene volume mixing ratios around the flux tower. Figure 5 shows the ratios of isoprene volume mixing ratios measured simultaneously at the tower and by the drone at a 30 m height. The average tower/drone ratios were 0.87 for the autumn observation at a horizontal distance of 15 m, 0.95 for the summer observation at 15 m, 1.32 for the summer observation at 30 m, and 0.99 for all data combined.The average values ± standard deviation of the ratio of isoprene volume mixing ratios obtained at the same time and height (30 m) from tower and drone observations (tower/drone) were plotted as shown in Fig. 7 to evaluate the variability in the horizontal direction. In autumn (horizontal distance between the tower and drone: 15 m), summer (15 m),

書式を変更: フォント : 斜体
書式を変更: 下付き
書式を変更: フォント : 斜体
書式を変更: 下付き
書式を変更: フォント : 斜体
書式を変更: 下付き
書式を変更: フォント : 斜体
書式を変更: 下付き
書式を変更: フォント : 斜体
書式を変更: 下付き
書式を変更: フォント : 斜体
書式を変更: 下付き
書式を変更: フォントの色 : 赤
書式を変更: 蛍光ペン (なし)

summer (30 m), and all data, the average values for tower/drone were 0.87, 0.95, 1.32, and 0.99, respectively. These results indicate that isoprene volume mixing ratios around the tower differed by approximately 10% within 15 m and by up to approximately 30% at 30 m under the sampled conditions.

Within a 15 m radius of the tower, the horizontal variation was approximately 10%, while at 30 m it was approximately 30%. In Japan, the standard for quality control in the measurement of air pollutants is generally defined as a difference of 30% or less between two or more measurement values obtained independently under the same conditions. As the volume mixing ratio differences due to horizontal variation of isoprene were generally within 30%, it was confirmed that there were no significant deviations.

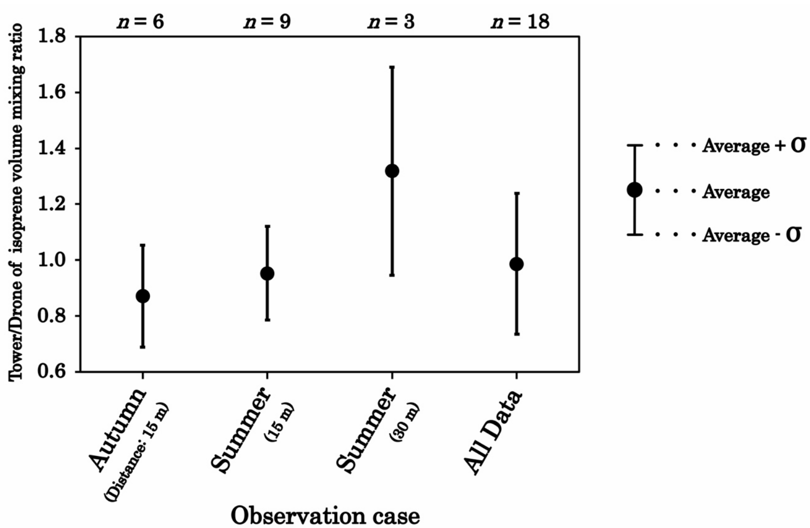


**Figure 57: Average and standard deviationRatios of isoprene volume mixing ratios measured simultaneously by the tower and drone at a 30 m height. Ratios are shown for the autumn observation at a 15 m horizontal distance, summer observations at 15 and 30 m horizontal distances, and all data combined. Points indicate average values, and error bars indicate ± standard deviation.observed at the same height and at the same time by tower and drone on days with different seasons and horizontal distances. The graphs in the figure show, from left to right, autumn (tower-drone distance: 15 m), summer (15 m), summer (30 m), and all data.**

The scatter plot between the drone and tower measurements is shown in Fig. 68. The slope of the regression line was 1.05, and the Pearson correlation coefficient was $r$ = 0.96 ($p$ < 0.001), suggesting that the drone-based sampling captured variations broadly consistent with the tower measurements. However, because the drone observations were limited to

**書式を変更:** 蛍光ペン (なし)

selected days and short sampling periods, the results should be interpreted as an assessment of short-range horizontal variability rather than as a general characterization of spatial heterogeneity at the site. The larger differences observed at a 30 m distance may reflect small-scale heterogeneity in canopy structure, leaf density, light environment, and turbulent transport. These results suggest that even within several tens of meters of a flux tower, horizontal variability can contribute to uncertainty in the interpretation of fixed-point BVOC observations.

書式を変更: フォントの色 : 自動

The scatter plot between the drone and tower measurements is shown in Fig. 8. The slope of the regression line was 1.05, and the Pearson correlation coefficient was $r = 0.96$ ($p < 0.001$), indicating a very strong positive correlation. This result shows that isoprene measurements taken by the drone are as accurate as those taken at the tower.

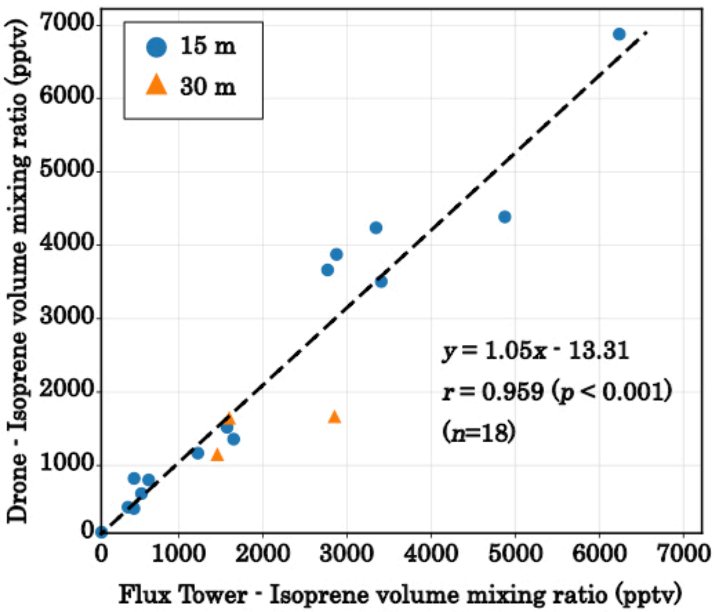


**Figure 68: Comparison of isoprene volume mixing ratios measured simultaneously by the tower and drone at a 30 m height. The regression line and correlation coefficient are shown for all paired data.Two-dimensional scatter plots of isoprene volume mixing ratios constructed using drone and tower measurements.**

As the distance increased, the volume mixing ratio difference between tower and drone samples grew larger. This difference could be attributed to increased isoprene emission intensity in summer, coupled with the impact of isoprene

~~emission heterogeneity caused by environmental variations such as temperature, light exposure, canopy density, and leaf density. Although drone flight times were limited, spatial variations were confirmed at locations distant from the tower.~~

### 3.4.2 Exploratory comparison of tower- and drone-derived flux estimates~~Horizontal variation of the isoprene flux~~

Figure 7~~9~~ shows the ratios of isoprene fluxes estimated from tower-based measurements at 23–30 m and drone-based measurements at 30–40 m. The average tower/drone flux ratios were 0.72, 0.98, and 0.85 for the 15 m, 30 m, and all-distance datasets, respectively. The all-distance dataset represents the combined 15 and 30 m drone sampling locations. ~~The scatter plot of all isoprene flux data ($n$ = 12) obtained from the tower and drone is shown in Fig. 10.~~~~the average values ± standard deviation of the isoprene flux ratio (tower/drone) obtained from observations at two different heights using a tower (23–30 m) and a drone (30–40 m). The average flux ratio between the tower and drone for horizontal distance differences of 15 m and 30 m across all data sets was 0.72, 0.98, and 0.85, respectively.~~ Under conditions of a horizontal distance of 30 m, the ~~average~~ flux ratios tended to approach 1 more than under conditions of 15 m. This indicates that the flux due to turbulent vertical transport is complex, and simply increasing the horizontal distance does not necessarily lead to ~~significantly~~ different values.

The scatter plot of tower- and drone-derived isoprene fluxes is shown in Fig. 8. ~~The scatter plot of all isoprene flux data ($n$ = 12) obtained from the tower and drone is shown in Fig. 10.~~ Although a positive correlation was observed between the two isoprene fluxes, it was not statistically significant when all data points were included ($y = 0.90x + 11.17$, $r = 0.44$, $p = 0.15$). However, when the two data points marked with black circles in the figure, which deviated significantly from the regression line, were excluded, the regression equation became $y = 0.67x + 7.74$, and $r = 0.74$ ($p = 0.015$), indicating a significant positive correlation between the two fluxes.

**書式を変更:** 蛍光ペン (なし)

**書式を変更:** 蛍光ペン (なし)

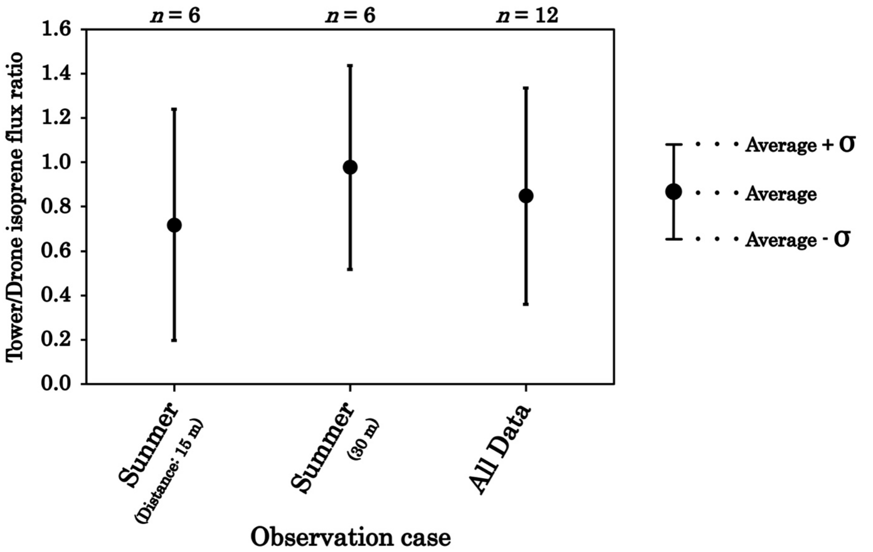


**Figure 79:** Ratios of tower-based and drone-based isoprene flux estimates during the supplemental drone experiment. Tower-based fluxes were calculated from the 23–30 m height interval, whereas drone-based fluxes were calculated from the 30–40 m height interval using tower-derived micrometeorological parameters. Points indicate average values, and error bars indicate ± standard deviation.Average and standard deviation of isoprene emission flux ratios observed simultaneously by tower and drone at different horizontal distances during summer. The two heights used for flux calculations based on the aerodynamic gradient method were 23 m and 30 m for the tower, and 30 m and 40 m for the drone. The graphs in the figure show, from left to right: summer (tower-drone distance: 15 m), summer (30 m), and all data.

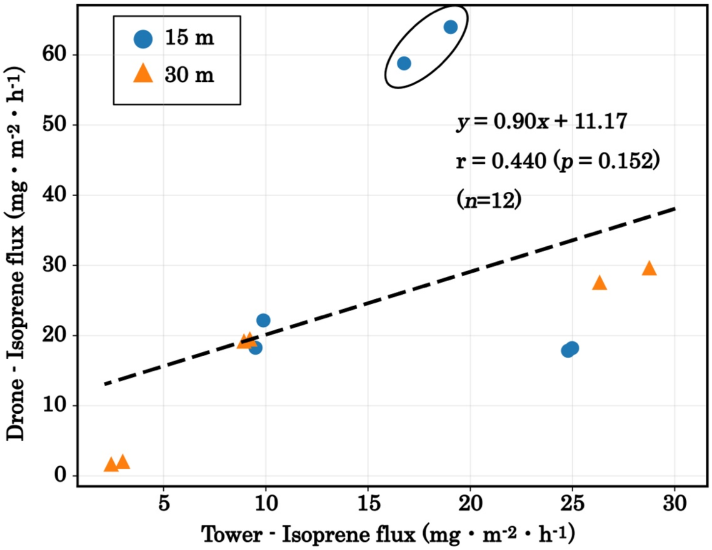


**Figure ~~10~~8: Exploratory comparison between tower-based and drone-based isoprene flux estimates. Tower-based fluxes were calculated from the 23–30 m height interval, whereas drone-based fluxes were calculated from the 30–40 m height interval using tower-derived micrometeorological parameters. The dashed line indicates the 1:1 relationship.~~Two-dimensional scatter plot of isoprene fluxes measured by drone and tower.~~ The two data points that deviate ~~significantly~~ from the regression line are marked with black circles.**

The comparison should be interpreted cautiously because the tower- and drone-derived fluxes were calculated from different height intervals and because the drone samples at 30 and 40 m were not collected simultaneously. In addition, micrometeorological parameters measured at the tower were used for the drone-based flux calculation because the drone could not carry a three-dimensional ultrasonic anemometer. Thus, the tower–drone flux comparison primarily reflects differences in concentration gradients, sampling height intervals, and sampling timing under tower-derived turbulence conditions, rather than directly measured differences in turbulent transport between the tower and drone locations. These methodological constraints likely contributed to the scatter in the tower–drone flux comparison. Accordingly, the drone-based flux analysis is treated here as an exploratory assessment of spatial representativeness and height-dependent uncertainty in gradient-based flux estimates. The results suggest that small-scale spatial variability and differences in sampling height can affect flux estimates, but additional observations are needed before this approach can be used for robust quantitative flux validation.~~Although the results regarding the isoprene volume mixing ratio ratio between the drone and the~~

tower, shown in Section 3.4.1, suggest that there are no major issues with the BVOC measurement method used for drones in this study, the following factors were considered to explain the major discrepancies observed in some of the flux ratio data. First, for safety reasons related to drone flight operations, the observation height could not be reduced below 30 m; therefore, the observation height for flux measurements using the drone could not be aligned with that of the tower. Second, while the tower can perform simultaneous sampling at two different heights, it is difficult for drones to carry out similar simultaneous sampling due to payload and equipment constraints. As a result, there is a time lag of approximately 10 min between sampling at 30 and 40 m. Third, since we were unable to install a 3-dimensional ultrasonic anemometer on the drone, we used data from the flux tower. These factors may contribute to the observed differences in flux ratios.

To the best of our knowledge, no known studies have previously estimated flux from drone observations between two heights. This approach was employed in the present study to evaluate the spatial representativeness of flux observations typically conducted on a single tower and the associated observational uncertainties, using actual measurement data. This study represents a novel approach and has yielded interesting results. However, as there is currently a lack of data for further verification, it will be necessary to continue accumulating and verifying measurement data on the spatial variability of fluxes in the future. Furthermore, as technology advances and improvements are made to drone payload limits and flight times through battery enhancements, it is expected that observations with even lower levels of uncertainty will be possible.

### 3.5 MEGAN comparison under the sampled conditionsmodel calculation results

#### 3.5.1 Characteristics and Vvariations in calculated fluxes of $F_{cal}$ and activity factors

Figure S9 shows the daily average MEGAN-calculated isoprene fluxes ($F_{cal}$) from June 1, 2023 to October 31, 2025. Daily averages were calculated from the 10 min model outputs during the daytime sampling window from 10:00 to 16:00. Figure 9 shows the monthly variations in $F_{cal}$ and the four activity factors $\gamma_{LAI}$, $\gamma_P$, $\gamma_T$, and $\gamma_{age}$ from June 2023 to October 2025. Monthly statistics are summarized in Table S4.

Figure S6 shows the monthly variations in the four activity factors $\gamma_{LAI}$, $\gamma_p$, $\gamma_T$, and $\gamma_{age}$, listed alongside $F_{cal}$ for the period from June, 2023, to October, 2025, derived from 10-min values between 10:00 AM and 4:00 PM. The time period was chosen to align with the actual observation period. Note that the period from 11:00 AM on December 1, 2023, to 3:30 PM on February 22, 2024, is treated as missing data due to power outages and equipment maintenance. Additionally, a table

書式を変更: 蛍光ペン (なし)

presenting monthly statistics for each year is provided as Table S3.

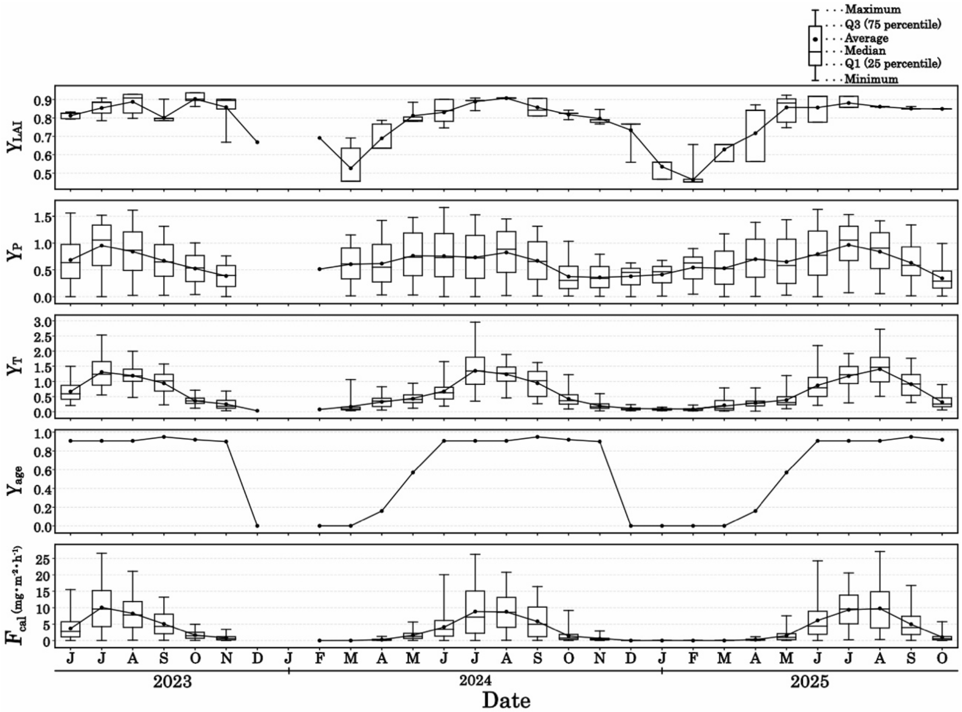


**Figure 9: Monthly variation in the overlay of average values on the boxplots of MEGAN-calculated isoprene fluxes $F_{cal}$ and the activity factors $\gamma_{LAI}$, $\gamma_P$, $\gamma_T$, and $\gamma_{age}$.**

The variation pattern of $F_{cal}$ , was generally which is low during the early spring leaf expansion period, increasedpeaking induring –summer, and– gradually decreasing decreased toward the autumn leaf-–fall period. This pattern reflects the combined effects of not only replicates the seasonal cycle corresponding to temperature, and light, LAI, and leaf age in the MEGAN algorithm.solar radiation variations, but also reflects the physiological seasonal cycle of *Q. serrata* through LAI and leaf age distribution, showing a tendency consistent with observed values. Focusing on the summer months season, which constitute theis the primary period for isoprene emission, this study calculates daily mean values limited to the 10:00 AM–4:00 PM time period. As a result, the "daytime peak" component represented by the model is emphasized compared to full-day averages, and the impact of high emission flux days is significantly amplified. the sSeasonal averages (median values) were 7.4 (6.1), 7.3 (5.7), and 8.5 (7.6) $\mathrm{mg\ m^{-2}\ h^{-1}}$ for 2023, 2024, and 2025, respectively. Among the sampled summers, the calculated daytime fluxes tended to be higher in 2025.. Over the three-year period, the model estimates showed the highest daily average flux in the summer of 2025, which is also consistent with the observed results.

$\gamma_{LAI}$ begins began to rise gradually around early spring in March, and from May to October, it generally remaineds saturated at aroundnear 0.8–0.9 from May to October. $\gamma_{P}$ $_{P}$ maintaineds a base level of around 0.4–0.5 even during winter and increased to, but rises to approximately 0.7–0.9 between June and August. $\gamma_{T}$ exhibits showed large seasonal variations, being very small atwith low values of around 0.1 during winter and , while reaching an average values of approximately 1.2–1.4 during July–August, suggesting it contributes significantly to the annual cycle $F_{cal}$. $\gamma_{age}$ begins to rise aroundincreased in spring, remaineds high from at around 0.9 from June through September, declineds slightly from October tothrough November, and droppeds to 0 during the leaf-fallfall season.

To quantitatively evaluate the relationship between $F_{cal}$ and $\gamma_{P}$, $\gamma_{T}$, Spearman's rank correlation coefficients ($r_s$) wereas calculated usingfrom the 10 -min data collected during the period from May to October, when isoprene emissions were levels are relatively high. As a result, tThe correlation coefficients were $\gamma_{P}$ ($r_s$=0.86 for $\gamma_{P}$ (, $p$<0.001) and 0.89 for $\gamma_{T}$ ($r_s$=0.89, $p$<0.001), indicating a very highstrong positive correlationrelationships. These relationships primarily reflect the structure of the MEGAN algorithm, in which light and temperature activity factors are major drivers of isoprene emission estimates under daytime conditions. This is consistent with physiological findings that isoprene emissions from leaves strongly depend on photosynthetic activity and temperature, supporting that MEGAN's algorithm for light and temperature response scheme in FM Tama appropriately captures the main temporal variation factors of the emission.

### 3.5.2 Comparison between observed and calculated fluxeson of $F_{obs}$ and $F_{cal}$

The comparison was performed using $F_{obs}$ and $F_{cal}$ for the period from May to October, when isoprene emission fluxes were most evidentare dominant, analyzing data from the observed days and time. The analysis period covered 24 d observationThe comparison included 24 observation days and 179 paired data points. As complete 10:00–16:00 observations were not available for all sampling days, the comparison was based only on available time-synchronized paired data. Gaps within the daytime sampling window may have increased the uncertainty of daily statistics because short-term variability within the day was not always fully captured. The data were summarized by season to examine whether model–observation differences varied among sampled phenological and meteorological conditions. As the number of paired data points differed among seasons, these seasonal statistics were used to describe model–observation differences within each sampled season rather than for evaluating complete seasonal model performance. The data comparison diagram is shown in Fig. 101, and statistical dataTable 2 summarizes the , MEBE and RMSE. are summarized in Table 2.

**書式を変更:** 蛍光ペン (なし)

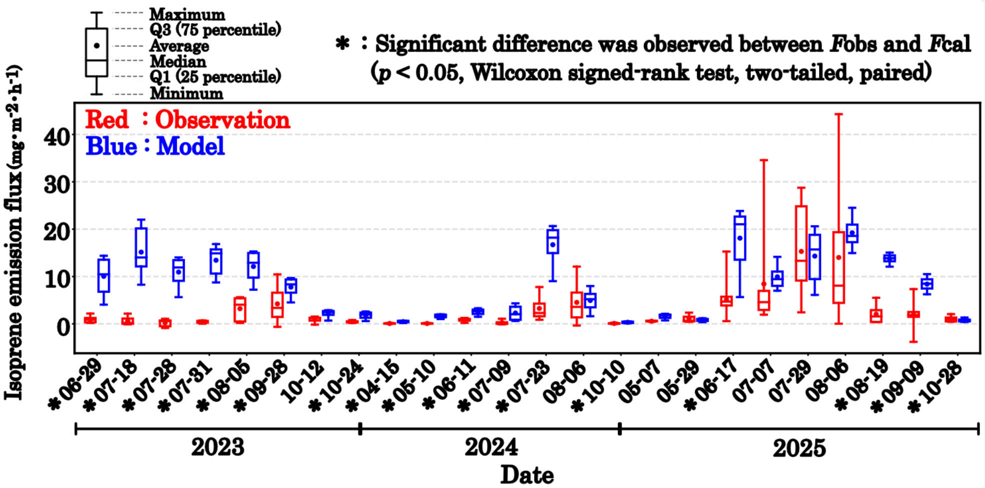


**Figure 10~~1~~: Comparison of observed tower-based isoprene fluxes (*$F_{obs}$*) and MEGAN-calculated fluxes (*$F_{cal}$*) for observation days from May to October. ~~Comparison of boxplots and average values for $F_{obs}$ and $F_{cal}$ on observation days during the period from May to October, when isoprene emissions are significant.~~**

**Table 2. Number of data points (*n*) used for the ~~comparative evaluation~~comparison between ~~of~~ $F_{obs}$ and $F_{cal}$ across ~~all~~ spring, summer, and autumn data, along with calculated results for mean ~~error~~ bias error (M~~E~~BE) and root mean square error (RMSE).**

| | *n* | M~~E~~BE[1)] | RMSE[1)] |
|---|---|---|---|
| ~~Spring~~May (Spring) | 22 | 0.80 | 1.11 |
| June–August (Summer)~~Summer~~ | 112 | 7.20 | 10.54 |
| September–October (Autumn)~~Autumn~~ | 45 | 2.16 | 3.76 |
| Overall | 179 | 5.15 | 8.56 |

1) unit: mg·m⁻²·h⁻¹

~~As the average F~~For the entire May–October dataset, $F_{cal}$ generally overestimated the $F_{obs}$, with ~~period (n=179),~~ M~~E~~BE=+5.15 mg·m$^{-2}$·h$^{-1}$ and RMSE=8.56 mg·m$^{-2}$·h$^{-1}$. The positive MBE indicates that MEGAN estimates were higher than observed fluxes on average under the sampled conditions.~~As MEB is positive, MEGAN showed a tendency to estimate flux higher than the observed values (overestimation).~~ The relatively large RMSE indicates that the model–observation differences cannot be explained solely by a uniform offset and likely reflect variability in environmental responses, canopy

書式を変更: フォント : 斜体
書式を変更: 下付き
書式を変更: フォント : 斜体
書式を変更: 下付き
書式付きの表
書式変更: インデント : 最初の行 : 10.63 字
書式を変更: Correspondence Char, フォントの色 : 自動
書式を変更: Correspondence Char, フォントの色 : 自動

representativeness, and observational flux uncertainty. ~~Given that the RMSE is also relatively large, when correcting MEGAN to match observed values, it is highly likely that unaccounted variability factors are influencing the results, which cannot be explained by a simple fixed subtraction.~~

The discrepancy between MEGAN and observations was largest during the summer observation period. The~~When decomposed by season,~~ M~~E~~BE and RMSE were +0.80 $\mathrm{mg\ m^{-2}\ h^{-1}}$ and 1.11 $\mathrm{mg\ m^{-2}\ h^{-1}}$ for spring ($n$=22), +7.20 $\mathrm{mg\ m^{-2}\ h^{-1}}$ and 10.54 $\mathrm{mg\ m^{-2}\ h^{-1}}$ for summer ($n$=112), and +2.16 $\mathrm{mg\ m^{-2}\ h^{-1}}$ and 3.76 $\mathrm{mg\ m^{-2}\ h^{-1}}$ for autumn ($n$=45), respectively~~, with summer showing particularly significant errors~~. Spring showed smaller MBE and RMSE, whereas summer showed the largest positive bias and scatter. Autumn showed smaller errors than summer, although a positive bias remained. These seasonal differences suggest that model–observation discrepancies were larger under the sampled high-temperature and high-light conditions, when $\gamma_T$ and $\gamma_P$ were relatively large. Possible causes include uncertainties in basal emission rates, canopy microclimate, foliar temperature, canopy-scale representativeness, and AGM-based observed fluxes. ~~The fact that trends differ by season is an important finding obtained through long-term observation in this study. Spring shows smaller MEB and RMSE, with MEGAN and observations relatively well-matched. Summer, however, exhibits the largest MEB and RMSE, featuring not only average overestimation but also likely containing discrepancies in the reproducibility of diurnal variations. Autumn shows reduced errors compared to summer; however, a positive bias persists. This seasonal difference is consistent with the strong light and temperature dependence of isoprene emissions. During summer, the effects of $\gamma_T$ and $\gamma_P$ become particularly pronounced, making it likely that discrepancies between the representativeness of the input and the actual foliar environment within the canopy are amplified as errors.~~

For each observation day, we evaluated the significance of daily distribution differences using the Wilcoxon signed-rank test (two-tailed, paired) with paired $F_{obs}$ and $F_{cal}$ data collected at the same time. The 22 d for which the number of daily pairs was at least five were included in the test. ~~The 22 d for which the number of daily pairs met the general threshold (5 or more) were included in the test.~~ The remaining two days (May 7, 2025, and May 29, 2025) were excluded from the test because they had only three~~3~~ pairs. The test results showed significant differences ($p$<0.05) on 17 of the 22 d. On 16 of those days, $F_{cal}$ tended to be higher than $F_{obs}$ ~~overestimate~~.

Seasonal ~~linear~~ regression analysis using time-synchronized paired data and daily averages ($F_{cal}$ = a × $F_{obs}$ + b) ~~is~~ is shown in Fig. S10~~12~~. For all seasons, the intercept was positive, suggesting that MEGAN tended to estimate non-negligible fluxes even when observed fluxes were low. ~~suggesting a tendency for MEGAN to assign a certain level of flux even under low observation conditions. Notably, t~~The summer intercept was particularly large, indicating a tendency toward ~~significant~~ overestimation in the low $F_{obs}$ range under the sampled summer conditions. Conversely, the slopes were ~~fell~~ below unity~~1~~ in ~~both~~ summer and autumn, suggesting that the model did not fully reproduce the observed range of flux variability under the sampled conditions.~~suggesting a relatively sluggish model response to increasing observations and potentially insufficient tracking of high emission events.~~ These results highlight the need for further evaluation of MEGAN parameterizations using canopy-scale observations in suburban forest environments.

**書式を変更:** フォント : 斜体

**書式を変更:** 下付き

**書式を変更:** フォント : 斜体

**書式を変更:** 下付き

**書式を変更:** 蛍光ペン (なし)

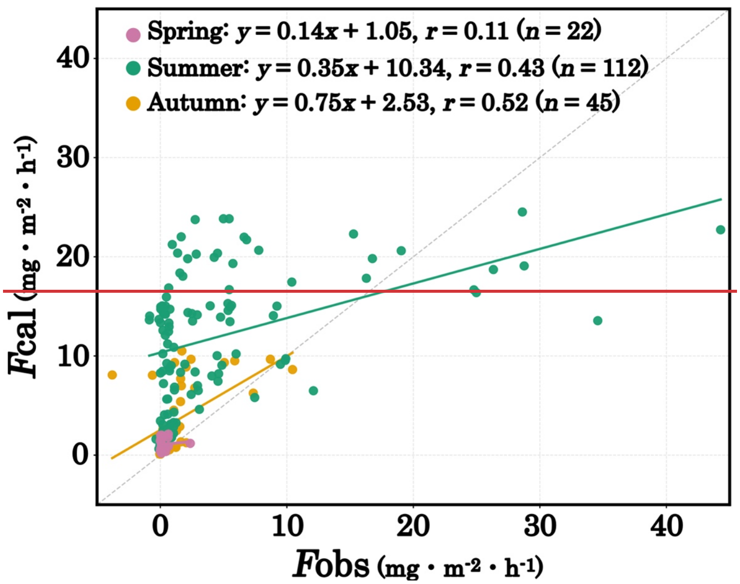


~~Figure 12: Scatter plot of $F_{obs}$ and $F_{cal}$. Pink circles indicate spring data, green circles indicate summer data, and orange circles indicate autumn data. The upper left shows the regression equations obtained by least squares fitting from the seasonal data.~~

## 4. Discussion

### 4.1. Environmental controls on isoprene fluxes under sampled daytime conditions ~~High isoprene emissions in summer 2025~~

The tower-based observations showed positive isoprene fluxes mainly during the warm-season sampling days, especially from June to September. The positive relationships between isoprene flux and canopy temperature, PPFD, and LAI indicate that the observed fluxes were influenced by temperature, light availability, and canopy development under the sampled daytime conditions. As the observations were conducted intermittently and did not cover complete diurnal cycles or all meteorological conditions, these relationships should be interpreted as tendencies within the sampled conditions rather than as a complete characterization of seasonal or interannual controls.

Isoprene production is strongly influenced by the availability of synthetic substrates, such as dimethylallyl diphosphate, generated through photosynthetic processes within chloroplasts, and by the activity of isoprene synthase. Photosynthesis depends on light availability, whereas isoprene synthase activity is strongly affected by temperature (Rasulov et al., 2010; Chen et al., 2022). Therefore, isoprene emissions are considered to correlate with temperature and PPFD. These physiological controls are consistent with the positive relationships observed between Fobs, canopy temperature, and PPFD in this study. However, according to Rasulov et al. (2010), the pool size of dimethylallyl diphosphate varies with temperature and decreases under high temperature conditions exceeding a threshold, suggesting that elevated temperatures may influence isoprene emission rates. Guenther et al. (1993) observed the relationship between isoprene emission and leaf temperature in isoprene emitting trees—Sweetgum, Eucalyptus, Aspen, and Velvet bean. They reported that, depending on the tree species, the emission peak occurred at approximately 35°C, with emission levels decreasing above approximately 40°C. Exceeding the threshold temperature is thought to be associated with the inactivation of the synthetic substrate. In this study, the highest canopy air temperatures (maximum of 35.7°C) during sampling approached this range. However, leaf temperature was not measured directly, and canopy air temperature was used as a proxy. Therefore, the possible occurrence of thermal optimum or high-temperature suppression cannot be evaluated quantitatively from the present data.

Leaf phenology also likely contributed to the observed flux variability. Young leaves generally have lower isoprene emission capacity than mature leaves (Kuzma and Fall, 1993), and *Q. serrata* at FM Tama develops new leaves in spring and maintains mature leaves during summer. The low fluxes observed in early spring are therefore consistent with the expected lower emission capacity of young leaves, whereas higher fluxes during summer are consistent with mature foliage and favorable light and temperature conditions. LAI showed a positive relationship with isoprene flux, although this relationship is expected to saturate when canopy light availability becomes limiting (Yu et al., 2017).

書式を変更: フォント : 斜体

Several high-flux events were observed during the summer 2025 sampling days.~~The summer of 2025 showed significantly higher isoprene emissions compared to the summers of 2023 and 2024, both in $F_{obs}$ and $F_{cal}$.~~ According to the Japan Meteorological Agency (2025), the 2025 rainy season ended earlier than usual, and in June and July, record-high temperatures were observed across northern, eastern, and western Japan, with the summer average temperature deviation reaching +2.36°C, significantly surpassing past records. This was attributed ~~due~~ to the Tibetan anticyclone extending over Japan as a result of the upper-level westerlies flowing northward from June onward, influenced by the early and active development of the Asian monsoon. Furthermore, the expansion of the Pacific anticyclone coincided with this, bringing clear skies and rising temperatures. Consequently, the cumulative number of locations recording daily maximum temperatures of 40°C or higher also set a new record.

The average temperatures at FM Tama between 10:00 and 16:00 during the summers of 2023, 2024 and 2025 were 31.96°C, 29.34°C and 33.19°C respectively.~~The average canopy temperatures at the FM Tama during the summers of 2023, 2024, and 2025 were 25.55°C, 25.81°C, and 26.32°C, respectively. When the average temperature at the time of observation was calculated, the figures for 2023, 2024, and 2025 were 31.96°C, 29.34°C, and 33.19°C, respectively, with 2025 recording the highest temperature across the 3 years.~~ Meanwhile, the average PPFD was not higher in 2025~~the average PPFD, another environmental factor contributing to isoprene flux intensity, during the summer observation period was 1,161, 1,095, and 1,021 μmol·m$^{-2}$·s$^{-1}$ in 2023, 2024, and 2025, respectively. Unlike temperature, the average PPFD was lowest in 2025, and it is believed that PPFD is not strongly correlated with the high increase in flux expected in 2025~~. Furthermore, no differences were observed in wind direction or wind speed among the observation days during the summer. This suggests that the high

Fobs values in 2025 were likely associated with high-temperature sampling conditions. However, because the number of sampling days was limited and meteorological conditions differed among observation days, the present dataset cannot separate interannual variability from day-to-day meteorological variability. Furthermore, there were no significant differences in wind direction and speed during the summer months over the 3-year period.

Previous studies have shown that warming and heat-wave conditions can enhance BVOC emissions and influence atmospheric chemistry.The average (rate of change) isoprene emissions in the summer of 2025 increased by +7.2 (360%) $mg \cdot m^{-2} \cdot h^{-1}$ for $F_{obs}$ and +1.2 (16%) $mg \cdot m^{-2} \cdot h^{-1}$ for $F_{cal}$ compared to the previous year. Kramshøj et al. (2016) reported enhanced BVOC emissions under experimental warming in a tundra ecosystem, although the climate and vegetation differ substantially from those at FM Tama.conducted a field experiment in the dry shrub tundra of West Greenland, where *Empetrum hermaphroditum* and the isoprene-emitting species *Salix glauca* co-dominate. Using the enclosure method, which involves enclosing the entire ecosystem plot (33 × 33 cm) comprising the vegetation and the underlying soil, the authors reported that when the temperature inside the enclosure was increased by an average of 3.1°C, BVOC emissions from the entire ecosystem increased by 260% compared with those in the control area. Although the tundra region differs in terms of climate and vegetation and, therefore, cannot be simply compared with Japan, which has a humid subtropical climate, the average temperature on the observation day in 2025 was approximately 1.23°C and 3.85°C higher than that in 2023 and 2024, respectively. Thus, it is possible that fluxes increased alongside temperature in 2025.

Figure 13 shows a scatter plot of summer isoprene flux and temperature inside canopy, plotted for each year. Even under the same high-temperature conditions, the flux varied significantly from year to year. The scatter plot shows that high fluxes were frequently observed in 2025 (approximately 32–35°C), and higher emissions were confirmed within this temperature range compared with those in 2023 and 2024.

書式変更: インデント : 最初の行 : 0 字

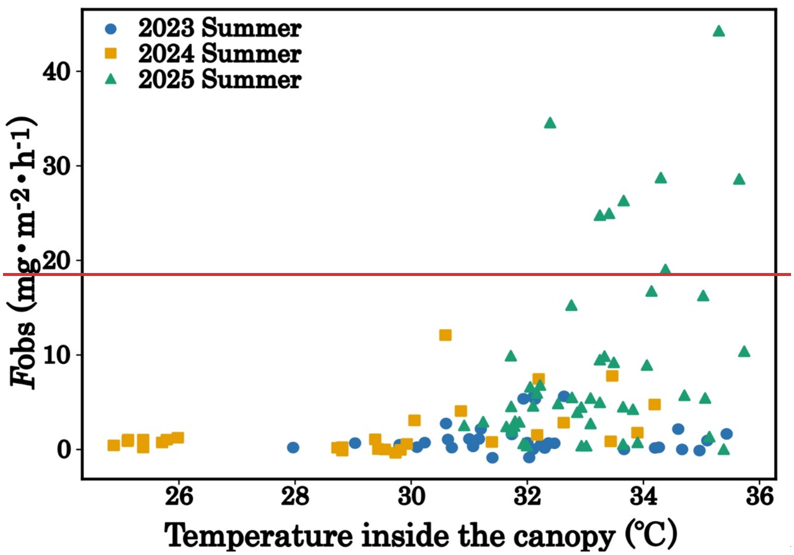


~~Figure 13: Two-dimensional scatter plot of isoprene emission flux and temperature inside the canopy for each summer. 2023 is indicated by blue circles, 2024 by orange squares, and 2025 by green triangles.~~

書式変更: インデント : 最初の行 : 0 字

~~The lower increase in $F_{cal}$ compared to $F_{obs}$ is thought to be due to the relatively sluggish response of MEGAN to high flux levels, as shown in Section 3.5.2, which results in insufficient tracking of high-emission events. In any case, we believe that the increase in isoprene emissions in 2025 was due to the unusually early end of the rainy season and rising temperatures, suggesting the influence of global warming and climate change. The ability to detect a significant upward trend in isoprene emissions under the climatic conditions in Japan in 2025, a year marked by record-breaking temperature rises due to the progression of global warming, was made possible by conducting interannual comparisons based on long-term observations.~~

Megaritis et al. (2013) predicted that a 2.5°C rise in temperature in Northern Europe would lead to an increase in BVOC emissions, resulting in a 20% increase in summer biogenic SOA. Moreover Churkina et al. (2017) estimated that increased BVOC emissions during heatwave events in the Berlin-Brandenburg metropolitan area of Germany contributed up to 60% ~~to~~ of $O_3$ formation, indicating that the impact of BVOC increases due to high temperatures on the atmospheric environment is significant. Furthermore, Wang et al. (2024) warn that during heat waves, plants not only increase the production of $O_3$ precursors but also close their stomata, thereby reducing $O_3$ removal by dry deposition~~thereby reducing the dry deposition of $O_3$ (making it harder to remove)~~; consequently, the increasing frequency of heat waves poses a major challenge for air pollution control. Therefore, continued BVOC flux observations under high-temperature conditions are important.

書式を変更: 下付き

Nevertheless, the present study should be regarded as providing observational evidence of high isoprene fluxes under selected hot daytime conditions, rather than a quantitative assessment of climate-change-driven trends in BVOC emissions.

書式を変更: フォントの色 : 赤, (言語 1) 日本語

書式変更: インデント : 最初の行 : 0 字

Due to global warming, high temperatures have persisted, and there are concerns that this trend will continue. Numerous observational and modeling studies indicate that temperature significantly contributes to BVOC emissions and predict increased isoprene emissions due to global warming (Okumura et al., 2008; Emmerson et al., 2020; Hata et al., 2023; Kramshøj et al., 2016). It is important to continue conducting thorough monitoring of BVOC emissions in response to changes in the global environment.

### 4.2. Spatial representativeness and uncertainty of supplemental drone observationsAnalysis of isoprene emission flux with temperature and PPFD

書式変更: インデント : 最初の行 : 1 字

The supplemental drone-based measurements provided information on short-range horizontal variability around the flux tower. The tower–drone comparison at a 30 m height indicated that isoprene volume mixing ratios differed by approximately 10% within 15 m and by up to approximately 30% at 30 m under the sampled conditions. These results suggest that even near a fixed flux tower, horizontal variability in canopy structure, leaf density, light environment, and turbulent transport can affect the interpretation of fixed-point BVOC observations.

However, the drone-based flux comparison should be interpreted with greater caution than the volume mixing ratio comparison. Drone-derived fluxes were calculated from the 30–40 m height interval, whereas tower-based fluxes were calculated from the 23–30 m height interval. In addition, the drone samples at 30 and 40 m were collected sequentially rather than simultaneously, and micrometeorological parameters measured at the tower were used because the drone could not carry a three-dimensional ultrasonic anemometer. Therefore, differences between tower- and drone-derived fluxes reflect not only horizontal variability in isoprene volume mixing ratios but also differences in the height interval, sampling timing, and assumed turbulence conditions.Observations in this study confirmed that temperature and PPFD significantly influence isoprene emission flux, consistent with previous research (Guenther et al., 1993; Bao et al., 2008). To examine these factors in combination, a 3-dimensional scatter plot of $F_{obs}$, temperature inside the canopy, and PPFD was created (Fig. S7). Under high temperature and high PPFD conditions, $F_{obs}$ tend to be high, but cases with low flux are also observed. This indicates that while temperature and light are the primary drivers, other factors may also govern flux variations, at least during certain periods and under specific conditions.

Future drone-based BVOC flux studies would benefit from simultaneous multi-height sampling and direct turbulence measurements on or near the drone platform. As drone payload capacity and flight endurance improve through advances in battery technology, longer sampling periods and the installation of additional micrometeorological sensors may become possible. These developments would help reduce uncertainties in drone-based BVOC flux estimates and strengthen their role as a complementary approach to tower-based observations.To analyze the factors involved, we first calculated the 75th percentile (Q3) for both temperature and PPFD from the entire observation dataset ($n$=263). We then extracted data points simultaneously satisfying temperature ≥ Q3 (approximately 32°C) and PPFD ≥ Q3 (approximately 1571 $\mu mol \cdot m^{-2} \cdot s^{-1}$). The $F_{obs}$ distribution of this subset ($n$=37, of which 36 were summer and 1 was autumn) was classified as follows. L-$F_{obs}$ denotes the group below the 25th percentile (approximately 1.5 $mg \cdot m^{-2} \cdot h^{-1}$, $n$=10), and corresponds to the data points marked with black circles in Fig. S7. Although we were unable to identify a clear cause for the occurrence of L-$F_{obs}$, factors unrelated to meteorological conditions, such as the spatial structure of the source distribution and the uneven distribution of unidentified shrubs and herbaceous plants, may play a crucial role.

**4.3 Possible causes of model–observation discrepancies in the MEGAN comparison4.3. Considerations on discrepancies between observed values and MEGAN calculations**

MEGAN generally overestimated the observed tower-based isoprene fluxes during the May–October sampling periods, with the largest MBE and RMSE during summer. As the comparison was based on time-synchronized paired data from intermittent daytime sampling, the results should be interpreted as model–observation differences under the sampled conditions rather than as a complete seasonal model evaluation. The larger summer discrepancy suggests that model uncertainties became more apparent under high-temperature and high-light conditions, when $\gamma_T$ and $\gamma_P$ were relatively large.

The larger summer discrepancy is important because summer is the period when isoprene emissions and photochemical activity are both enhanced. In urban and suburban environments, uncertainty in BVOC emission estimates can influence simulations of $O_3$ and SOA formation, where biogenic precursors interact with anthropogenic nitrogen oxides. Therefore, reducing model–observation discrepancies under summer high-temperature and high-light conditions is important for improving BVOC emission estimates and their application to air quality modeling.MEGAN overestimated observed values during spring, summer, and autumn, where isoprene emissions were detected. Particularly during summer, when BVOC emissions are high and contribute to $O_3$ and SOA formation, reducing the discrepancy with observed values is crucial for developing atmospheric environmental countermeasures and strategies and constructing future predictions.

Both the observed fluxes and the MEGAN estimates include substantial uncertainties. The observed fluxes were estimated using the AGM, which depends on the measured concentration gradient, eddy diffusivity, stability correction, displacement height, and the assumption that the selected measurement heights were within a layer of approximately constant flux (Erisman and Draaijers 1995). In forest canopies, especially within or near the roughness sublayer, this assumption can be difficult to fully satisfy. Chemical loss or transformation of reactive BVOCs within and above the canopy may also influence the relationship between their emission and measured flux. Therefore, part of the model–observation discrepancy may reflect uncertainty in the observed flux estimates themselves.

Uncertainty in the basal emission rate ($\varepsilon$) is another likely source of discrepancy. MEGAN uses PFT-based standard emission factors, but these values may not fully represent the dominant species and local canopy conditions at FM Tama. Langford et al. (2017) raised concerns that $\varepsilon$ in MEGAN was calculated based on a very limited number of leaf-level

**書式を変更:** フォント : 斜体
**書式を変更:** 下付き
**書式を変更:** フォント : 斜体
**書式を変更:** 下付き
**書式を変更:** 下付き
**書式を変更:** 蛍光ペン (なし)
**書式を変更:** フォント : 斜体 (なし)

observations, resulting in considerable uncertainty. Tani et al. (2024) also emphasized that differences in measurement methods can cause variability in reported $\varepsilon$ even for the same species. For *Q. serrata*, Okumura et al. (2008) reported leaf-level basal emission rates of 42.9 nmol $m^{-2}$ $s^{-1}$ for sunlit leaves and 20.5 nmol $m^{-2}$ $s^{-1}$ for shaded leaves. These values indicate that the emission capacity of *Q. serrata* can differ substantially between different leaf light environments. In the present study, we used the PFT-based standard emission factor in MEGAN to provide a baseline comparison with the tower-based flux observations. A full sensitivity analysis and validation using species-specific and sun/shade-specific emission factors would require additional assumptions regarding canopy structure, leaf area distribution, sunlit and shaded leaf fractions, and scaling from leaf-level emission capacity to canopy-scale fluxes. Such an analysis is therefore beyond the scope of the present study, but it represents an important next step for improving the MEGAN evaluation at this site.

The temperature response factor $\gamma_T$ may also contribute to the discrepancy. In the present study, $F_{cal}$ showed strong relationships with $\gamma_T$ and $\gamma_P$, reflecting the structure of the MEGAN algorithm. Previous studies suggest that temperature response parameterizations may vary among ecosystems and species. Emmerson et al. (2020) measured isoprene using the leaf cuvette method across four Eucalyptus species at temperatures ranging from 293–328 K in 5 K increments, reporting that the temperature-dependent peak occurred at higher temperatures than those reported in the original MEGAN study. DiMaria et al. (2023) argued that ecosystem-specific $\gamma_T$ parameterizations are needed to improve the representation of temperature sensitivity. At FM Tama, the high-temperature summer sampling conditions may have amplified uncertainties in the temperature response function and In the representativeness of canopy air temperature for leaf temperature.

Canopy-scale representativeness of the input variables is another important issue. MEGAN was driven by observed meteorological variables and LAI, but the actual foliar environment within the canopy can vary vertically and horizontally. Sunlit and shaded leaves experience different light and temperature conditions, and these differences may not be fully represented by tower-level PPFD, air temperature, or local LAI measurements. The drone observations also indicated short-range horizontal variability in isoprene volume mixing ratios near the tower. These factors may partly explain why a uniform correction to MEGAN is insufficient to reproduce the observed flux variability.~~Guenther et al. (2012) estimated the uncertainty in isoprene emission from MEGAN to be approximately on a factor of two. Emmerson et al. (2016) found that MEGAN overestimated isoprene flux by a factor of three compared to observations obtained using PTR-MS and eddy covariance flux measurements for eucalypt species known as high isoprene emitters in southeastern Australia. Given that uncertainties differing by several factors or orders of magnitude would inevitably lead to significant discrepancies from reality, both observational data and model calculations inherently involve uncertainty, making perfect agreement impossible. However, identifying the causes of these discrepancies and taking steps to address them hold academic importance.~~

Overall, the MEGAN comparison in this study should be interpreted as an evaluation under intermittent daytime sampling conditions. The results indicate potential sources of model–observation discrepancy, including basal emission factors, temperature response functions, canopy microclimate, spatial representativeness, and AGM-based flux uncertainty. However, because the observations were limited to selected daytime periods, the comparison does not represent a complete seasonal or

- **書式を変更:** フォント : 斜体
- **書式を変更:** 上付き
- **書式を変更:** 上付き
- **書式を変更:** 上付き
- **書式を変更:** 上付き
- **書式を変更:** フォント : 斜体
- **書式を変更:** フォント : 斜体
- **書式を変更:** 下付き
- **書式を変更:** フォント : 斜体
- **書式を変更:** 下付き
- **書式を変更:** フォント : 斜体
- **書式を変更:** 下付き
- **書式を変更:** フォント : 斜体
- **書式を変更:** 下付き
- **書式を変更:** フォント : 斜体
- **書式を変更:** 下付き
- **書式を変更:** フォントの色 : テキスト 1

annual model evaluation.Regarding spatial uncertainty in tower observations, we verified horizontal variation in both isoprene volume mixing ratio and flux. For horizontal variation of isoprene volume mixing ratio with relatively similar sampling conditions, volume mixing ratio variations within a 15–30 m radius of the tower were found to be within 30%. Although the uncertainty in the flux was expected to be higher due to differences in measurement height relative to that of the tower caused by safety considerations for the drone, as well as limitations on micro-meteorological factors on the drone side, it remained within 30%. These results indicate that spatial uncertainty of this magnitude is to be expected.

The basal emission rate ($\varepsilon$) assigned in MEGAN based on plant functional type (PFT) serves as the foundation for model estimation, but Langford et al. (2017) raised concerns that it was calculated based on a very limited number of leaf-level observations, resulting in extremely high uncertainty. Tani et al. (2024) summarized past leaf-level measurement data and highlighted that differences in measurement methods can cause variation in $\varepsilon$ even within the same tree species. Furthermore, Geron et al. (2000) studied the seasonal variability of $\varepsilon$ in multiple leaves of white oak (*Quercus alba L.*) under standard conditions of the G93 model, reporting that it fluctuated significantly throughout the summer and also exhibited diurnal variation of approximately two-fold. Additionally, Okumura et al. (2008) conducted field observations using the leaf cuvette method on mature *Q. serrata* in the forests of Yamashiro, Kyoto. They found that the $\varepsilon$ at the leaf level for sunlit leaves was 42.9 nmol·m$^{-2}$·s$^{-1}$, while shaded leaves showed a rate of 20.5 nmol·m$^{-2}$·s$^{-1}$. Therefore, $\varepsilon$ is considered to possess an extremely complex nature. In MEGAN, changes in emission due to seasonally varying weather, leaf phenology, and environmental conditions are structured to be scaled by $\gamma$. However, based on these prior studies, it may be necessary to consider factors such as environmental conditions, region, and seasonality for $\varepsilon$ as well, rather than treating it as a fixed value throughout the year.

書式を変更: フォントの色 : 赤

As confirmed in this study, because the activity factors $\gamma$ exhibit a particularly pronounced positive correlation response with emission flux, especially with respect to $\gamma_T$, they may also significantly contribute to the uncertainty. Emmerson et al. (2020) measured isoprene using the leaf cuvette method across four Eucalyptus species at temperatures ranging from 293–328 K in 5 K increments, reporting that the temperature-dependent peak occurs at higher temperatures than in the original MEGAN study. DiMaria et al. (2023) argue that developing $\gamma_T$ parameterizations optimized for each ecosystem is necessary to accurately model the temperature sensitivity of isoprene emission. Previous studies on the emission characteristics of BVOC under high-temperature conditions did not consider evaluating sensitivity of native plant species to $\gamma_T$ due to advancing climate warming. Furthermore, in calculating activity factors $\gamma$, a significant amount of empirical data established during the MEGAN development process has been utilized. It would be worthwhile to verify whether these values truly represent the optimal values for each region.

書式を変更: フォントの色 : 赤

## 5. Summary and cConclusion

This study conducted intermittent multi-year, multi-height BVOC observations at a 30 m flux tower in a suburban Tokyo forest dominated by Quercus serrata under a humid subtropical climate. Isoprene fluxes were estimated using the aerodynamic gradient method (AGM), and supplemental drone-based measurements were conducted on selected days to examine short-range horizontal variability around the tower. The observed tower-based fluxes were also compared with MEGAN estimates to evaluate model–observation agreement under the sampled daytime conditions. BVOC samples were collected at four heights, 30, 23, 17, and 3 m above ground level, during 34 sampling days from June 2023 to October 2025.The key features of this study are the long-term, multi-height BVOC observations using a flux tower and isoprene flux measurements using the aerodynamic gradient method (AGM) in a research forest (a mixed forest dominated by *Quercus serrata*) in the suburbs of Tokyo, which has a humid subtropical climate. Additionally, we evaluated the spatial variability of isoprene through integrated observations with drone and assessed the reproducibility of MEGAN. The observation period lasted approximately two and a half years, from June 2023 to October 2025. Multi-height BVOC observations were conducted at four heights: 30 m, 23 m, 17 m, and 3 m above ground level.

The tower observations showed that the volume mixing ratios of the target BVOCs were generally low during the cold-season sampling days (November–April), whereas those of isoprene increased markedly during warm-season sampling days (May–October). During peak summer observations, isoprene accounted for more than 90% of the measured BVOC composition. Isoprene volume mixing ratios were generally highest at 17 m, corresponding to the canopy layer, and higher values were also observed at 23 and 30 m above the main canopy during warm-season sampling. These vertical profiles indicate that enhanced isoprene volume mixing ratios were frequently observed within the *O. serrata* canopy and that isoprene emitted from the canopy was transported upward. In contrast, monoterpene volume mixing ratios remained much lower than those of isoprene, and clear vertical gradients were not evident. These results indicate that isoprene was the dominant BVOC under the sampled warm-season daytime conditions at this site.

Tower-based isoprene fluxes estimated by AGM ranged from −0.05 to 15.30 mg m$^{-2}$ h$^{-1}$ on a daytime daily average basis. Positive fluxes were mainly observed during warm-season sampling days, especially from June to September. Several high-flux events were observed during summer 2025, when canopy temperatures during sampling were relatively high. However, because the observations were intermittent and meteorological conditions differed among sampling days, these differences should be interpreted as variations under sampled summer conditions rather than as evidence of an interannual trend. Isoprene fluxes showed positive relationships with canopy temperature, PPFD, and LAI, indicating that temperature, light availability, and canopy development were important controls on the observed fluxes under the sampled daytime conditions.

The supplemental drone-based measurements provided information on short-range horizontal variability around the tower. At a 30 m height, tower–drone comparisons showed that isoprene volume mixing ratios differed by approximately 10% within a horizontal distance of 15 m and by up to approximately 30% at 30 m under the sampled conditions. These results suggest that even within several tens of meters of a flux tower, small-scale variability in canopy structure, light environment, and turbulent transport can influence the interpretation of fixed-point BVOC observations. Drone-derived flux estimates were also examined using the 30–40 m height interval, but these estimates should be regarded as exploratory because turbulence was not measured at the drone sampling points, the tower and drone used different height intervals, and the drone

**書式を変更:** フォント : 斜体

**書式を変更:** 上付き

**書式を変更:** 上付き

samples at 30 and 40 m were not collected simultaneously. Therefore, these drone measurements are interpreted as a supplementary approach for evaluating spatial representativeness and methodological uncertainty, rather than as an independent validation of tower-based fluxes.

The comparison between tower-based $F_{obs}$ and MEGAN-calculated $F_{cal}$ during May–October included 24 observation days and 179 time-synchronized paired data points. MEGAN generally overestimated the observed fluxes under the sampled conditions, with an overall MBE of +5.15 mg m$^{-2}$ h$^{-1}$ and RMSE of 8.56 mg m$^{-2}$ h$^{-1}$. The discrepancy was largest during summer, when the MBE and RMSE were +7.20 and 10.54 mg m$^{-2}$ h$^{-1}$, respectively. This larger summer discrepancy is important because isoprene emissions and photochemical activity are both enhanced under warm and high-light conditions, and uncertainties in BVOC emission estimates can influence simulations of $O_3$ and SOA formation in urban and suburban environments. Possible causes of the model–observation discrepancy include uncertainties in the basal emission rate, temperature and light response factors, canopy microclimate, foliar temperature, canopy-scale representativeness, and AGM-based observed fluxes.

As the observations were intermittent and limited to selected daytime periods, this study does not provide a complete diurnal, seasonal, or interannual characterization of BVOC emissions at FM Tama. Monthly, seasonal, and annual differences should therefore be interpreted as tendencies under sampled daytime conditions rather than as complete climatological patterns or long-term trends. Despite these limitations, this study demonstrates the potential and limitations of combining multi-height tower observations, supplemental drone-based sampling, and MEGAN comparison to evaluate BVOC fluxes and their spatial representativeness in a suburban forest environment. Future work should include more continuous tower-based BVOC flux measurements, direct turbulence measurements during drone sampling, simultaneous multi-height drone sampling, and sensitivity tests using *Q. serrata* specific basal emission rates and canopy microclimate information. Such improvements would help reduce uncertainties across leaf, canopy, and landscape scales and improve the use of BVOC observations for emission model evaluation and air quality modeling.Observations from the tower revealed that during the cold season (November–April), each BVOC component was present at low volume mixing ratios with small vertical differences. In contrast, during the warm season (May–October), isoprene volume mixing ratios surged dramatically, accounting for over 90% of the BVOC composition in July and August. Vertically, isoprene volume mixing ratios peaked at 17 m, corresponding to the canopy layer. During the warm season, the volume mixing ratio difference between the canopy layer and the above-canopy layer increased, forming a distinct vertical gradient. This confirmed that the primary source of isoprene is within the canopy, and that emitted isoprene is transported upward by turbulent transport. In contrast, monoterpenes generally remained at low volume mixing ratios throughout the year, and the vertical gradient was not distinct. Long-term data confirmed that isoprene is the dominant BVOC at this site.

Isoprene emission flux calculated by AGM ranged from −0.05 to 15.30 mg·m$^{-2}$·h$^{-1}$ on a daily average basis, with a seasonal pattern showing a peak during summer. The seasonal average (median) for summer (June–August) was notably higher in 2025 at 9.2 (5.2) mg·m$^{-2}$ ·h$^{-1}$, compared to 1.2 (0.6) mg·m$^{-2}$ ·h$^{-1}$ in 2023 and 2.0 (1.0) mg·m$^{-2}$ ·h$^{-1}$ in 2024. The high emission flux in 2025 is considered to be due to the historically high temperatures recorded that year. This result

書式を変更: フォント : 斜体
書式を変更: 下付き
書式を変更: フォント : 斜体
書式を変更: 下付き
書式を変更: 上付き
書式を変更: 上付き
書式を変更: 下付き
書式を変更: フォント : 斜体

suggests that annual isoprene emission may increase as temperatures rise with future global warming. The relationship between isoprene flux and environmental factors revealed a significant positive relationship with temperature inside the canopy, PPFD, and LAI, clearly demonstrating that emissions are controlled by temperature, sunlight, and leaf area (phenology).

Regarding spatial variability assessment through integrated tower and drone observations, horizontal heterogeneity near the tower was quantified. The volume mixing ratio of tower/drone at the same height (30 m) and time showed an average of approximately 0.87–0.95 at a horizontal distance of 15 m. This can be summarized as approximately 10% variation at the 15 m scale. However, at a distance of 30 m, the average was 1.32, indicating that the heterogeneity expanded to approximately 30% at the 30 m scale. This heterogeneity was more pronounced during the warm season, suggesting that under conditions of active isoprene emissions, differences in tree species composition, microtopography, and canopy structure are reflected in volume mixing ratio patterns. Moreover, to the best of our knowledge, this study represents the first observational attempt to estimate isoprene flux between two heights using drone-based measurements. The estimated flux agreed with the tower-based flux within approximately 30% at a horizontal distance of 30 m.

Comparing flux tower observations with MEGAN revealed a clear tendency for the model to consistently overestimate observed flux values. Simultaneous comparisons from May to October ($n$=179) yielded MEB=+5.15 and RMSE=8.56 $mg \cdot m^{-2} \cdot h^{-1}$. When examined seasonally, the errors followed the order summer > autumn > spring. During summer, MEB=+7.20 and RMSE=10.54, with overestimation becoming particularly pronounced during periods of high emission conditions. This divergence suggests that basal emission rate ($\varepsilon$), temperature response ($\gamma_T$), light response ($\gamma_P$), leaf area ($\gamma_{LAI}$) and other factors may not sufficiently match site-specific conditions. Furthermore, it indicates that uncertainties stemming from spatial variability on the observational side are also present.

To more accurately characterize the impacts of BVOC on global environmental systems such as air quality, climate, and the carbon cycle under conditions of advanced global warming, further observations and quantitative analyses of BVOC emissions are necessary. Future research priorities for this work include re-evaluating site-specific $\varepsilon$ and activity factors $\gamma$, as well as verifying alternative estimation models. Furthermore, the incorporation of multi-point aerial observations using drone has yielded promising results. Progress in observationally constraining horizontal and vertical heterogeneity is expected to contribute to improving the reliability of evaluating canopy-scale spatial variability of BVOCs and reducing uncertainties in regional emission inventories and air quality predictions.

**Code and data availability**

The BVOC data observed in this study and the computational data from the MEGAN model are available from the JPCOAR Cloud site (https://cess.repo.nii.ac.jp/records/200000~~0~~12~~3~~), a repository constructed and operated by the Japan Consortium for Open Access Repository (Open Access Repository Promotion Association).

**Author contributions**

YI: Conceptualization, Data curation, Formal analysis, Funding acquisition, Investigation, Methodology, Project administration, Software, Validation, Visualization, Writing – original draft. KY: Investigation, Writing – review and editing. SY: Conceptualization, Funding acquisition, Methodology, Writing – review and editing. KT: Resources, Writing – review and editing. AS: Supervision, Writing – review and editing. KM: Resources, Supervision, Writing – review and editing. TO: Conceptualization, Funding acquisition, Methodology, Supervision, Writing – review and editing.

**Competing interests**

The contact author has declared that none of the authors has any competing interests.

**Disclaimer**

Publisher's note: Copernicus Publications remains neutral with regard to jurisdictional claims made in the text, published maps, institutional affiliations, or any other geographical representation in this paper. The authors bear the ultimate responsibility for providing appropriate place names. Views expressed in the text are those of the authors and do not necessarily reflect the views of the publisher.

**Acknowledgements**

Drone flight was assisted by Mr. Yuji Yamamoto and Mr. Hiroto Watanabe of Green Blue Co., Ltd. We would like to express our gratitude to them.

**Financial support**

This work was supported by Japan Society for the Promotion of Science KAKENHI (grant number 23K11413).

**References**

Altamira-Colado, E., Cuevas-González, D., Reyna, M. A., García-Vázquez, J. P., Avitia, R. L., and Osornio-Vargas, A. R.: Drone-assisted particulate matter measurement in air monitoring: A patent review, Atmosphere, 15, 515, https://doi.org/10.3390/atmos15050515, 2024.

Atkinson, R., and Arey, J.: Atmospheric degradation of volatile organic compounds, Chem. Rev., 103, 4605–4638. https://doi.org/10.1021/cr0206420, 2003.

Bai, J., Guenther, A. B., Turnipseed, A., Duhl, T., Yu, S., and Wang B.: Seasonal variations in whole-ecosystem BVOC emissions from a subtropical bamboo plantation in China, Atmos. Environ., 124, 12–21, https://doi.org/10.1016/j.atmosenv.2015.11.008, 2016.

Bai, J., Wu, Z., Yang, C., and Guenther, A.: Seasonal variations in whole–ecosystem BVOC emissions and ozone fluxes from a tropical rubber tree plantation in China, Atmos. Environ., 351, 121182, https://doi.org/10.1016/j.atmosenv.2025.121182, 2025.

Baker, B., Bai, J. H., Johnson, C., Cai, Z. T., Li, Q. J., Wang, Y. F., Guenther, A., Greenberg, J., Klinger L., Geron, C., Rasmussen, R.: Wet and dry season ecosystem level fluxes of isoprene and monoterpenes from a southeast Asian secondary forest and rubber tree plantation, Atmos. Environ., 39, 381–390, https://doi.org/10.1016/j.atmosenv.2004.07.033, 2005.

~~Bao, H., Kondo, A., Kaga, A., Tada, M., Sakaguti, K., Inoue, Y., Shimoda, Y., Narumi, D., and Machimura, T. (2008). Biogenic volatile organic compound emission potential of forests and paddy fields in the Kinki region of Japan, Environ. Res., 106, 156–169, https://doi.org/10.1016/j.envres.2007.09.009, 2008.~~

Bouvier-Brown, N. C., Schade, G. W., Misson, L., Lee, A., Mckay, M., and Goldstein, A. H.: Contributions of biogenic volatile organic compounds to net ecosystem carbon flux in a ponderosa pine plantation, Atmos. Environ., 60, 527–533, https://doi.org/10.1016/j.atmosenv.2012.06.070, 2012.

~~Celedon, J. M., and Bohlmann, J.: Oleoresin defenses in conifers: chemical diversity, terpene synthases and limitations of oleoresin defense under climate change, New Phytol., 224, 1444–1463, https://doi.org/10.1111/nph.15984, 2019.~~

Chatani, S., Matsunaga, S. N., and Nakatsuka, S.: Estimate of biogenic VOC emissions in Japan and their effects on photochemical formation of ambient ozone and secondary organic aerosol, Atmos. Environ., 120, 38–50, https://doi.org/10.1016/j.atmosenv.2015.08.086, 2015.

~~Chatani, S., Kokubu, Y., Takahashi, K., and Hoshi, J.: Validation of emission inventories and air quality simulations based on concentrations of individual VOC species measured in Tokyo, J. Jpn. Soc. Atmos. Environ., 57, 35–52, https://doi.org/10.11298/taiki.57.35, 2022.~~

Chen, Y.-J., Huang, Y.-L., Chen, Y.-H., Chang, S.-T., and Yeh, T.-F.: Biogenic volatile organic compounds and protein expressions of *Chamaecyparis formosensis* and *Chamaecyparis obtusa* var. formosana leaves under different light intensities and temperatures, Plants, 11, 1535. https://doi.org/10.3390/plants11121535, 2022.

Churkina, G., Kuik, F., Bonn, B., Lauer, A., Grote, R., Tomiak, K., and Butler, T. M.: Effect of VOC emissions from vegetation on air quality in Berlin during a heatwave, Environ. Sci. Technol., 51, 6120–6130, https://doi.org/10.1021/acs.est.6b06514, 2017.

DiMaria, C. A., Jones, D. B. A., Worden, H., Bloom, A. A., Bowman, K., Stavrakou, T., Miyazaki, K., Worden, J., Guenther, A., Sarkar, C., Seco, R., Park, J-H., Tota, J., Alves, E. G., and Ferracci, V.: Optimizing the isoprene emission model MEGAN with satellite and ground-based observational constraints, J. Geophys. Res., 128, e2022JD037822, https://doi.org/10.1029/2022JD037822, 2023.

Dumont, C., Verreyken, B. W. D., Schoon, N., Bergmans, B., Heinesch, B., and Amelynck, C.: Multi-year observations of BVOCs and ozone: concentrations and fluxes measured above and below the canopy in a mixed temperate forest, Earth Syst. Sci. Data, 18, 617-654, https://doi.org/10.5194/essd-18-617-2026, 2026.

Emmerson, K. M., Galbally, I. E., Guenther, A. B., Paton-Walsh, C., Guerette, E.-A., Cope, M. E., Keywood, M. D., Lawson, S. J., Molloy, S. B., Dunne, E., Thatcher, M., Karl, T., and Maleknia, S. D.: Current estimates of biogenic emissions from eucalypts uncertain for southeast Australia, Atmos. Chem. Phys., 16, 6997–7011, https://doi.org/10.5194/acp-16-6997-2016, 2016.

**書式を変更:** 蛍光ペン (なし)

Emmerson, K. M., Possell, M., Aspinwall, M. J., Pfautsch, S., and Tjoelker, M. G.: Temperature response measurements from eucalypts give insight into the impact of Australian isoprene emissions on air quality in 2050, Atmos. Chem. Phys., 20, 6193-6206, https://doi.org/10.5194/acp-20-6193-2020, 2020.

EPA: https://www.epa.gov/sites/default/files/2019-12/documents/to-15a_vocs.pdf, last access: 29 April 2026.

Erisman, J. W., and Draaijers, G. P. J.: Atmospheric deposition in relation to acidification and eutrophication, Studies in Environmental Research 63, Elsevier, The Netherlands, 55–71, 1995.

Fares, S., Schnitzhofer, R., Jiang, X., Guenther, A., Hansel, A., and Loreto, F.: Observations of diurnal to weekly variations of monoterpene-dominated fluxes of volatile organic compounds from mediterranean forests: implications for regional modeling, Environ. Sci. Technol., 47, 11073–11082, https://doi.org/10.1021/es4022156, 2013.

Fuentes J. D. and Wang, D.: On the seasonality of isoprene emissions from a mixed temperate forest, Ecol. Appl., 9, 1118–1131, https://doi.org/10.1890/1051-0761(1999)009[1118:OTSOIE]2.0.CO;2, 1999.

Fuentes, J. D., Wang, D., and Gu, L.: Seasonal variations in isoprene emissions from a boreal aspen forest, J. Appl. Meteorol. Climatol., 38, 855–869, https://doi.org/10.1175/1520-0450(1999)038<0855:SVIIEF>2.0.CO;2, 1999.

~~Geron, C., Guenther, A., Sharkey, T., and Arnts, R. R.: Temporal variability in basal isoprene emission factor, Tree Physiol., 20, 799–805, https://doi.org/10.1093/treephys/20.12.799, 2000.~~

Guenther, A. B., Zimmerman, P. R., Harley, P. C., Monson, R. K., and Fall, R.: Isoprene and monoterpene emission rate variability: Model evaluations and sensitivity analyses, J. Geophys. Res., 98, 12609–12617, https://doi.org/10.1029/93JD00527Digital Object Identifier, 1993.

Guenther, A., Hewitt, C. N., Erickson, D., Fall, R., Geron, C., Graedel, T., Harley, P., Klinger, L., McKay, W. A., Pierce, T., Scholes, B., Steinbrecher, R., Tallamraju, R., Taylor, J., and Zimmerman, P.: A global model of natural volatile organic compound emissions, J. Geophys. Res., 100, 8873–8892, https://doi.org/10.1029/94JD02950, 1995.

Guenther, A., Baugh, B., Brasseur, G., Greenberg, J., Harley, P., Serca, D., Vierling, L.: Isoprene emission estimates and uncertainties for the central African EXPRESSO study domain, J. Geophys. Res., 104 (D23), 30625–30639. https://doi.org/10.1029/1999JD900391, 1999.

Guenther, A. B., Karl, T., Harley, P., Wiedinmyer, C., Palmer, P. I., and Geron, C.: Estimates of global terrestrial isoprene emissions using MEGAN (Model of Emissions of Gases and Aerosols from Nature), Atmos. Chem. Phys., 6, 3181–3210, https://doi.org/10.5194/acp-6-3181-2006, 2006.

Guenther, A. B., Jiang, X., Heald, C. L., Sakulyanontvittaya, T., Duhl, T., Emmons, L. K., Wang, X.: The Model of Emissions of Gases and Aerosols from Nature version 2.1 (MEGAN2.1): an extended and updated framework for modeling biogenic emissions, Geosci. Model Dev., 5, 1471–1492, https://doi.org/10.5194/gmd-5-1471-2012, 2012.

~~Guenther, A. B.: Biological and chemical diversity of biogenic volatile organic emissions into the atmosphere, ISRN Atmospheric Sciences, 2013, 786290, http://dx.doi.org/10.1155/2013/786290, 2013.~~


書式を変更: 下線なし

書式を変更: 下線なし

書式を変更: 下線なし

Hata, H., Inoue, K., Yoshikado, H., Genchi, Y., and Tsunemi, K.: Impact of introducing net-zero carbon strategies on tropospheric ozone ($O_3$) fine particulate matter ($PM_{2.5}$) concentrations in Japanese region in 2050, Sci. Total Environ., 891, 164442, https://doi.org/10.1016/j.scitotenv.2023.164442, 2023.

Hayashi, K.: Atmospheric deposition 4. atmosphere-land exchange of substances, J. Jpn. Soc. Atmos. Environ. 45, A21-A31, 2010.

Holzinger, R., Lee, A., McKay, M., and Goldstein A. H.: Seasonal variability of monoterpene emission factors for a ponderosa pine plantation in California, Atmos. Chem. Phys., 6, 1267-1274, https://doi.org/10.5194/acp-6-1267-2006, 2006.

Ieda, T., Kitamori, Y., Mochida, M., Hirata, R., Hirano, T., Inukai, K., Fujinuma, Y., and Kawamura, K.: Diurnal variations and vertical gradients of biogenic volatile and semi-volatile organic compounds at the Tomakomai larch forest station in Japan, Tellus. Ser. B, Chem. Phys. Meteorol., 58, 177–186, https://doi.org/10.1111/j.1600-0889.2006.00179.x, 2006.

Ichikawa, Y., Nojiri, K., and Sasaka, K.: Determination of BVOCs based on high time-resolved measurements in urban and forest areas in Japan, Asian j. atmospheric environ., 17, 10, https://doi.org/10.1007/s44273-023-00009-6, 2023.

IPCC: https://www.ipcc.ch/report/ar6/wg1/, last access: 29 April 2026.

Japan Meteorological Agency: https://www.jma.go.jp/jma/press/2509/05b/kentoukai20250905.html, last access: 29 April 2026.

Jutti, S.: Monoterpene emission rate measurements from a Monterey Pine, J. Geophys. Res., 95, 7515-7519, https://doi.org/10.1029/JD095iD06p07515, 1990.

Kramshøj, M., Vedel-Petersen, I., Schollert, M., Rinnan, Å., Nymand, J., Ro-Poulsen, H., & Rinnan, R.: Large increases in Arctic biogenic volatile emissions are a direct effect of warming, Nat. Geosci., 9, 349–352, https://doi.org/10.1038/NGEO2692, 2016.

Kuzma, J., and Fall, R.: Leaf isoprene emission rate is dependent on leaf development and the level of isoprene synthase, Plant Physiol., 101, 435–440, https://doi.org/10.1104/pp.101.2.435, 1993.

Langford, B., Cash, J., Acton, W. J. F., Valach, A. C., Hewitt, C. N., Fares, S., Goded, I., Gruening, C., House, E., Kalogridis, A.-C., Gros, V., Schafers, R., Thomas, R., Broadmeadow, M., and Nemitz, E.: Isoprene emission potentials from European oak forests derived from canopy flux measurements: an assessment of uncertainties and inter-algorithm variability, Biogeosciences, 14, 5571–5594, https://doi.org/10.5194/bg-14-5571-2017, 2017.

Matsuda, K., Fujimura, Y., Hayashi, K., Takahashi, A., and Nakaya, K.: Deposition velocity of PM2.5 sulfate in the summer above a deciduous forest in central Japan, Atmos. Environ., 44, 4582–4587, https://doi.org/10.1016/j.atmosenv.2010.08.015, 2010.

Matsuda, K., Watanabe, I., Mizukami, K., Ban, S., and Takahashi, A.: Dry deposition of $PM_{2.5}$ sulfate above a hilly forest using relaxed eddy accumulation, Atmos. Environ., 107, 255–261, https://doi.org/10.1016/j.atmosenv.2015.02.050, 2015.

McKinney K. A., Lee, B. H., Vasta, A., Pho, T. V., and Munger, J. W.: Emissions of isoprenoids and oxygenated biogenic volatile organic compounds from a New England mixed forest, Atmos. Chem. Phys., 11, 4807–4831, https://doi.org/10.5194/acp-11-4807-2011, 2011.


**書式を変更:** 蛍光ペン (なし)

McKinney, K. A., Wang, D., Ye, J., de Fouchier, J.-B., Guimarães, P. C., Batista, C. E., Souza, R. A. F., Alves, E. G., Gu, D., Guenther, A. B., and Martin, S. T.: A sampler for atmospheric volatile organic compounds by copter unmanned aerial vehicles, Atmos. Meas. Tech., 12, 3123-3135, https://doi.org/10.5194/amt-12-3123-2019, 2019.

Megaritis, A. G., Fountoukis, C., Charalampidis, P. E., Pilinis, C., and Pandis, S. N.: Response of fine particulate matter concentrations to changes of emissions and temperature in Europe, Atmos. Chem. Phys., 13, 3423–3443, https://doi.org/10.5194/acp-13-3423-2013, 2013.

Miyama, T., Okumura, M., Kominami, Y., Yoshimura, K., Ataka, M. and Tani A.: Nocturnal isoprene emission from mature trees and diurnal acceleration of isoprene oxidation rates near *Quercus serrata* Thunb. Leaves, J. For. Res., 18, 93–97, https://doi.org/10.1007/s10310-012-0350-5, 2013.

Mochizuki, T., Tani, A., Takahashi, Y., Saigusa, N., and Ueyama, M.: Long-term measurement of terpenoid flux above a *Larix kaempferi* forest using a relaxed eddy accumulation method, Atmos. Environ., 83, 53–61, https://doi.org/10.1016/j.atmosenv.2013.10.054, 2014.

Mochizuki, T., Miyazaki, Y., Ono, K., Wada, R., Takahashi, Y., Saigusa, N., Kawamura, K., and Tani, A.: Emissions of biogenic volatile organic compounds and subsequent formation of secondary organic aerosols in a Larix kaempferi forest, Atmos. Chem. Phys., 15, 12029–12041, https://doi.org/10.5194/acp-15-12029-2015, 2015.

Mochizuki, T., Takanashi, S., Wada, R., Miyazaki, Y., Nakano, T., & Tani, A.: Canopy fluxes of monoterpene, isoprene and isoprene oxidation products in a pine-oak forest. J. Agric. Meteorol., 76, 36–43. https://doi.org/10.2480/agrmet.D-19-00039, 2020.

Muñoz-Sabater, J., Dutra, E., Agustí-Panareda, A., Albergel, C., Arduini, G., Balsamo, G., Boussetta, S., Choulga, M., Harrigan, S., Hersbach, H., Martens, B., Miralles, D. G., Piles, M., Rodríguez-Fernández, N. J., Zsoter, E., Buontempo, C., and Thépaut, J.-N.: ERA5-Land: a state-of-the-art global reanalysis dataset for land applications, Earth Syst. Sci. Data, 13, 4349–4383, https://doi.org/10.5194/essd-13-4349-2021, 2021.

Naemura, A., Yoshikawa, T., Satoh, K., and Dokiya, Y.: Measurements of throughfall and stem-flow of *Cryptomermeria japonica* in Oku-chichibu and Tama Hills. Jpn. J. Biometeror., 39, 121–125, https://doi.org/10.11227/seikisho.39.121, 2003.

Ninkovic, V., Markovic, D., and Rensing, M.: Plant volatiles as cues and signals in plant communication, Plant Cell Environ., 44, 1030–1043, https://doi.org/10.1111/pce.13910, 2020.

Nishimura, H., Shimadera, H., Kondo, A., Akiyama, K., and Inoue, Y.: Numerical analysis on biogenic emission sources contributing to urban ozone concentration in Osaka, Japan, Asian j. atmospheric environ, 9, 259–271, https://doi.org/10.5572/ajae.2015.9.4.259, 2015.

Okumura M, Tohno S, Tani A, Kominami Y, Miyama T, Takanashi S, and Kosugi Y: Isoprene emission characteristics of Quercus serrata in a deciduous broad-leaved forest. J. Agric. Meteorol., 64, 49–60, https://doi.org/10.2480/agrmet.64.49, 2008.

Okumura, M.: Environmental factors affecting the emission of volatile organic compounds from vegetation, Earozoru Kenkyu, 36, 19–24, https://doi.org/10.11203/jar. 36.19, 2021.

書式を変更: 蛍光ペン (なし)

書式を変更: 蛍光ペン (なし)

書式を変更: 蛍光ペン (なし)

書式を変更: 蛍光ペン (なし)

Penuelas, J., and Llusià, J.: Plant VOCs emissions: making use of the unavoidable, Trends Ecol. Evol., 19, 402–404, https://doi.org/10.1016/j.tree.2004.06.002, 2004.

Räisänen, T., Ryyppö, A., and Kellomäki, S.: Monoterpene emission of a boreal Scots pine (Pinus sylvestris L.) forest, Agric. For. Meteorol., 149, 808–819, https://doi.org/10.1016/j.agrformet.2008.11.001, 2009.

Rantala, P., Järvi, L., Taipale, R., Laurila, T. K., Patokoski, J., Kajos, M. K., Kurppa, M., Haapanala, S., Siivola, E., Petäjä, T., Ruuskanen, T. M., and Rinne, J.: Anthropogenic and biogenic influence on VOC fluxes at an urban background site in Helsinki, Finland, Atmos. Chem. Phys., 16, 7981–8007, https://doi.org/10.5194/acp-16-7981-2016, 2016.

書式を変更: 蛍光ペン (なし)

Rasulov, B., Hüve, K., Bichele, I., Laisk, A., and Niinemets, Ü.: Temperature response of isoprene emission in vivo reflects a combined effect of substrate limitations and isoprene synthase activity: a kinetic analysis. Plant Physiol., 154, 1558–1570, https://doi.org/10.1104/pp.110.162081, 2010.

Seco, R., Karl, T., Turnipseed, A., Greenberg, J., Guenther, A., Llusia, J., Peñuelas, J., Dicken, U., Rotenberg, E., Kim, S., and Yakir, D.: Springtime ecosystem-scale monoterpene fluxes from Mediterranean pine forests across a precipitation gradient, Agric. For. Meteorol., 237, 150–159. https://doi.org/10.1016/j.agrformet.2017.02.001, 2017.

書式を変更: 蛍光ペン (なし)

~~Sharifi, R., and Ryu, C. M.: Social networking in crop plants: wired and wireless cross-plant communications, Plant Cell Environ., https://doi.org/10.1111/pce.13966, 2020.~~

Sharkey, T. D., Wiberley, A. E., and Donohue, A. R.: Isoprene emission from plants: why and how, Ann. Bot., 101, 5–18, https://doi.org/10.1093/aob/mcm240, 2008.

Situ, S., Guenther, A., Wang, X., Jiang, X., Turnipseed, A., Wu, Z., Bai, J., and Wang, X.: Impacts of seasonal and regional variability in biogenic VOC emissions on surface ozone in the Pearl River delta region, China, Atmos. Chem. Phys., 13, 11803–11817, https://doi.org/10.5194/acp-13-11803-2013, 2013.

Tani, A., and Kawawata, Y.: Isoprene emission from the major native Quercus spp. in Japan, Atmos. Environ., 42, 4540–4550, https://doi.org/10.1016/j.atmosenv.2008.01.059, 2008.

Tani, A., and Mochizuki, T.: Review: Exchanges of volatile organic compounds between terrestrial ecosystems and the atmosphere, J. Agric. Meteorol., 77, 66–80, https://doi.org/10.2480/agrmet.D-20-00025, 2021.

Tani, A., Masui, N., Chang, T. W., Okumura, M., and Kokubu, Y.: Basal emission rates of isoprene and monoterpenes from major tree species in Japan: interspecies and intraspecies variabilities, Prog. Earth Planet. Sci., 11, 42, https://doi.org/10.1186/s40645-024-00645-8, 2024.

Wang, H., Nagalingam, S., Welch, A. M., Leong, C., Czimczik, C. I., and Guenther, A. B.: Heat waves may trigger unexpected surge in aerosol and ozone precursor emissions from sedges in urban landscapes, PNAS, 121, e2412817121, https://doi.org/10.1073/pnas.2412817121, 2024.

Wei, D., Fuentes, J.D., Gerken, T., Chamecki, M., Trowbridge, A. M., Stoy, P.C., Katul, G.G., Fisch, G., Acevedo, O., Manzi, A., von Randow, C, and dos Santos, R. M. N.: Environmental and biological controls on seasonal patterns of isoprene above a rain forest in central Amazonia, Agric. For. Meteorol., 256-257, 391–406, https://doi.org/10.1016/j.agrformet.2018.03.024, 2018.

Xu, M., Kasahara, K., Sorimachi, A., and Matsuda, K.: Nitric acid dry deposition associated with equilibrium shift of ammonium nitrate above a forest by long-term measurement using relaxed eddy accumulation, Atmos. Environ., 256, 118454, https://doi.org/10.1016/j.atmosenv.2021.118454, 2021.

Yang, W., Cao, J., Wu, Y., Kong, F., and Li, L.: Review on plant terpenoid emissions worldwide and in China, Sci. Total Environ., 787, 147454, https://doi.org/10.1016/j.scitotenv.2021.147454, 2020.

Yu, H., Guenther, A., Gu, D., Warneke, C., Geron, C., Goldstein, A., Graus, M., Karl, T., Kaser, L., Misztal, P., and Yuan, B.: Airborne measurements of isoprene and monoterpene emissions from southeastern U.S. forests, Sci. Total Environ., 595, 1498–1511, https://doi.org/10.1016/j.scitotenv.2017.03.262, 2017.

**書式を変更:** 下線なし